

**ION TRAP MASS SPECTROMETRY: ON-LINE ELECTROCHEMISTRY  
AND IMPROVED ION DETECTION EFFICIENCY**

**By**

**JON ALLEN JONES**

**A DISSERTATION PRESENTED TO THE GRADUATE SCHOOL  
OF THE UNIVERSITY OF FLORIDA  
IN PARTIAL FULFILLMENT OF THE REQUIREMENTS FOR THE  
DEGREE OF DOCTOR OF PHILOSOPHY**

**UNIVERSITY OF FLORIDA**

**1995**

To my beloved wife, Michelle.

## ACKNOWLEDGEMENTS

I wish to express my gratitude to Dr. Richard A. Yost for his guidance during the completion of this work. I would also like to acknowledge and thank the members of my graduate committee, Dr. James Winefordner, Dr. Merle Battiste, Dr. Joseph Delfino, and Dr. Willard Harrison.

I would also like to thank the U.S. Environmental Protection Agency, Environmental Research Labs (Duluth, MN) and Environmental Monitoring Systems Labs (Cincinnati, OH) for their financial support of this work.

I thank my fellow group members, especially Nathan Yates and Donald Eades, for their assistance with software and instrumentation, in addition to Jodie Johnson, Brad Coopersmith, Ulrich Bernier, and John Laycock.

Finally, I would like to express my deepest gratitude to my wife for standing by me these many years to provide support and comfort. I cannot fully express the great asset Michelle has been for me over the past six years I have been at UF, but through good times and bad she has always been there for me.

# TABLE OF CONTENTS

	<u>page</u>
ACKNOWLEDGEMENTS.....	iii
ABSTRACT.....	vi
CHAPTERS	
1 INTRODUCTION.....	1
Electrochemistry/Mass Spectrometry.....	2
Quadrupole and Quadrupole Ion Trap Mass Spectrometry.....	6
Tandem Mass Spectrometry.....	11
Thermospray Interface.....	18
Particle Beam Interface.....	19
Overview of Dissertation.....	21
2 EXAMINING THE OXIDATION OF AROMATIC AMINES BY ON-LINE ELECTROCHEMISTRY/ THERMOSPRAY/MASS SPECTROMETRY.....	22
Introduction.....	22
Electrochemical Equipment.....	23
Mass Spectrometer.....	23
Mass Spectrometric Hydrodynamic Voltammograms.....	25
Off-line Electrochemistry.....	26
On-line Electrochemistry.....	31
Conclusions.....	39
3 PARTICLE BEAM/ION TRAP MASS SPECTROMETRY FOR THE INVESTIGATION OF AROMATIC AMINES USING ON-LINE ELECTROCHEMISTRY.....	40
Introduction.....	40
Particle Beam Interface.....	41
Mass Spectrometers.....	44
Electrochemistry/Particle Beam/ITMS.....	64
Electrochemistry/Particle Beam/ITS40.....	79
Conclusions.....	86

4	IMPROVED ION DETECTION EFFICIENCIES FOR IONS STORED IN A QUADRUPOLE ION TRAP.....	89
	Introduction.....	89
	Experimental.....	90
	Characterization of Detection by Rapid Removal of RF.....	92
	Comparison of Rapid Removal of RF and Mass-Selective Instability Scanning.....	113
	Further Improvements.....	116
	Conclusions.....	124
5	CONCLUSIONS AND FUTURE WORK.....	126
	LITERATURE CITED.....	132
	BIOGRAPHICAL SKETCH.....	135

Abstract of Dissertation Presented to the Graduate School  
of the University of Florida in Partial Fulfillment  
of the Requirements for the Degree of Doctor of Philosophy

ION TRAP MASS SPECTROMETRY: ON-LINE ELECTROCHEMISTRY AND  
IMPROVED ION DETECTION EFFICIENCY

by

Jon Allen Jones

August 1995

Chairman: Richard A. Yost  
Major Department: Chemistry

An electrochemical cell is interfaced on-line with both quadrupole and ion trap mass spectrometers for the study of the environmental degradation of aromatic amines. Two types of liquid chromatography interfaces are used to accomplish on-line electrochemistry: a thermospray interface is used with the quadrupole mass spectrometer and a particle beam interface is used with the ion traps. This on-line system allows the electrochemical products to be monitored directly as the potential applied to the cell is varied. The use of on-line monitoring also allows for detection of products in a shorter time period than would be possible using bulk electrolysis and off-line monitoring. The use of EC/MS/MS using a quadrupole ion trap is

demonstrated in this work for the first time. Benzidine exhibited tendencies to form methoxy-substituted amines when a methanol mobile phase was used at low flow rates. The anilines formed dimers in either methanol or aqueous phases with primary amines dimerizing through the formation of azo- and hydrazo-derivatives, while tertiary amines dimerized through linkage between the rings.

The dissertation also presents a study of a new method of effecting ion ejection from an ion trap mass spectrometer for ion detection. Upon rapid removal of the RF trapping field all ions stored in the ion trap become unstable and are ejected. The application of a positive DC voltage to the ring electrode is shown to greatly enhance the detected ion signal for this ejection scheme. When the standard method of ion ejection, mass-selective instability scanning, is compared with ejection by rapid removal of the RF it is observed that rapid removal of RF produces as much as fifty times greater ion signal under the same conditions for ion creation and storage.

## CHAPTER 1 INTRODUCTION

In this dissertation two areas of research are presented: utilizing electrochemistry on-line with mass spectrometry for the investigation of degradative pathways of environmental pollutants and improving ion detection efficiencies in a quadrupole ion trap by rapid removal of the RF trapping field. The use of different interfaces (particle beam and thermospray) for combining the solution-phase electrochemistry with the high-vacuum of a mass spectrometer will be discussed. In addition, two types of mass spectrometers (triple quadrupole mass spectrometer and a quadrupole ion trap) will be examined. Comparison of results of off-line electrochemistry and on-line electrochemistry/mass spectrometry, of results from different interfaces for electrochemistry/mass spectrometry, and of the different mass spectrometers used in electrochemistry/mass spectrometry will be presented. Finally, a method of improving the detected ion signal in an ion trap will be presented along with implications of this technique for use in mass spectrometry applications directed toward environmental screening.

In this introductory chapter, some background on electrochemistry/mass spectrometry (EC/MS) will be presented, including previous research utilizing this technique. A discussion of the principles of operation of the particle beam and thermospray interfaces will be presented. Theory of operation of the triple



quadrupole and quadrupole ion trap mass spectrometers will also be discussed, with a somewhat more detailed examination of the theory of quadrupole ion traps being given. Finally, an overview of the organization of this dissertation will be given.

### Electrochemistry/Mass Spectrometry

Examining the fate of environmental contaminants or assessing the mutagenic potential of a compound generally requires some type of biological testing. This testing may involve soil microbes or small animals but is in any case time consuming and costly. Since the reactions that occur in living systems to alter chemicals (i.e., metabolism) are generally oxidation or reduction, methods to model environmental degradation or metabolism can be based on electrochemical behavior.

Methods have been demonstrated which use biologically-derived components, specifically enzymes, to effect the transformations of chemical species to model metabolism [1-3]. In these experiments, enzymes are immobilized on a chromatography column to allow on-line chemical modification of solution-phase species. The enzyme reactors are efficient and selective, and have been shown to be effective in protein sequencing applications [1,2] and metabolism studies of purine compounds [3].

Electrochemistry has been shown to yield similar reactive intermediates and products to enzymatic reactions [4-7]. Isolating and identifying reaction intermediates and products after an off-line electrochemical reaction is often a difficult process due to the many reactions that may occur during the time prior to

analysis. It is therefore preferable to analyze the electrochemically generated products as soon as possible after their formation; this is most effectively accomplished through the use of electrochemistry on-line with the detection scheme, in this case, mass spectrometry.

Bruckenstein was the first to combine electrochemistry on-line with mass spectrometry [8]. In this work a porous Teflon membrane acted as the solution-phase interface to the mass spectrometer; the interface design is shown in Figure 1.1. Volatile components of the mixture, such as carbon dioxide or oxygen, could pass through the membrane while the membrane acted as a barrier for the transfer of liquid phase components to the mass spectrometer. Bruckenstein used this system to monitor generation of oxygen from 0.1 M perchloric acid [8], production of methanol via the oxidation of methoxyphenols [9], and formation of ammonia from the reduction of nitrate [10]. Results from the initial experiments with oxygen generation indicated that 36% of the oxygen generated entered the mass spectrometer vacuum system through the membrane. Further experiments using Teflon membranes and silicone membranes were performed by other groups with some success [11,12]; however, the basic approach of using a membrane to separate the solution phase from the mass spectrometer vacuum phase limits the analyses to volatile electrochemical reactants and products which can permeate through the membrane material.

An interface was needed to allow the introduction of nonvolatile, polar species common in electrochemistry; this interface was provided with the invention

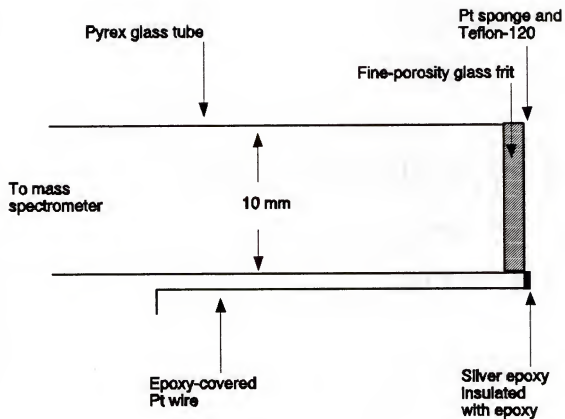


Figure 1.1

Diagram of the membrane probe used to monitor volatile products in electrochemistry/mass spectrometry [8].

of the thermospray (TSP) interface by Vestal [13]. Hambitzer and Heitbaum first used the thermospray interface to perform on-line EC/MS, examining the oxidation of N,N-dimethylaniline by monitoring the formation of dimers and trimers [14]. The system used in these experiments still allowed a relatively long time for reactions to occur after the compound was no longer in contact with the electrode due to an approximately 10 s dead time between generation of the electrochemical product and detection in the mass spectrometer. The products observed are consistent with mechanisms proposed for the oxidation of DMA [15,16].

Volk, Toth, and Yost have used electrochemistry on-line with mass spectrometry and tandem mass spectrometry using a thermospray interface for the elucidation of redox reactions of purines and pyrimidines [17]. The oxidation of uric acid was examined using EC/TSP/MS, and reaction intermediates identified. In these experiments, the dead time between the electrochemical cell and the mass spectrometer was reduced to approximately 500 ms; therefore, short-lived electrochemical intermediates could be examined. By using tandem mass spectrometry, structural information about electrochemically generated species was obtained. Furthermore, the use of MS/MS provides information on individual electrochemical products and intermediates within the reaction mixture without chromatographic separation [17].

To compare mass spectrometric results with off-line cyclic voltammetry, Volk developed the mass spectrometric hydrodynamic voltammogram (MSHV) [17]. The concept of this experiment is that the mass spectrum will be examined as the

potential applied to the EC cell is varied in a controlled manner; the potential is not scanned as in CV, rather the MSHV is composed of data obtained by injection of the sample at several different potentials. By plotting the intensities of particular  $m/z$  ions of interest against the applied potential, a voltammogram is derived which uses selected ion intensities rather than electrochemical current. A MSHV obtained for uric acid is shown in Figure 1.2 [17].

Electrochemistry has also been used on-line with thermospray/mass spectrometry to enhance the spectra of difficult to ionize species [20]. This research used the electrochemistry to transform a compound into a species which was more amenable to thermospray. Electrochemically assisted FAB has also been demonstrated [21].

### Quadrupole and Quadrupole Ion Trap Mass Spectrometry

The quadrupole mass filter and the quadrupole ion trap were first introduced by Paul in the 1950s [22]. Both operate on the basic principle of containing ions of specific mass to charge ratios ( $m/z$ ) in stable trajectories through the application of radio-frequency (RF) and direct current (DC) voltages to a set of electrodes to form a hyperbolic field. The quadrupole mass filter, or simply quadrupole, is a device consisting of four rods of hyperbolic (or round) cross-section to which these voltages are applied. The quadrupole ion trap is the three-dimensional analogue of the quadrupole consisting of a hyperbolic ring electrode to which these voltages are applied and two hyperbolic endcap electrodes; ions are

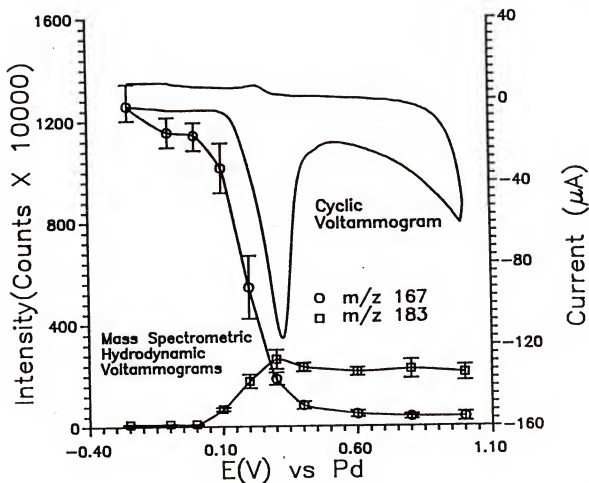


Figure 1.2

Mass spectrometric hydrodynamic voltammogram of uric acid [17]; shown are mass chromatograms for  $m/z$  167,  $(M-H)^-$  of uric acid, and  $m/z$  183,  $(M-H)^-$  of imine alcohol product. Also shown is the off-line cyclic voltammogram.

contained in a region in space where their trajectories are stable, that is, the ions do not strike an electrode surface.

Quadrupole mass filters are scanning devices. The applied RF and DC voltages are ramped, under computer control, in a manner such that ions of increasing mass-to-charge ratios sequentially pass through the filter to the detector. During the scan, the ratio of RF to DC is held constant as the voltages are ramped. The stability of ions is described by Mathieu theory which relates the motion of ions of particular mass-to-charge values to the applied RF and DC voltages [23]. Ionization, mass analysis, and detection occur in different regions of space.

Quadrupole ion traps are composed of three electrodes; a ring electrode and two endcap electrodes. The regions of stability within an ion trap are also described by Mathieu theory which relates ion motion to the applied voltages [23]. Most commonly a stability diagram based on Mathieu theory is used to illustrate circumstances which result in stable or unstable ion motion. Stability diagrams describe the combinations of RF and DC voltages which result in ions of a particular mass-to-charge having stable trajectories; each value of mass-to-charge has its own stability diagram in RF-DC space. For convenience, stability diagrams are often constructed in terms of the dimensionless quantities  $a$  and  $q$  which relate to the applied DC and RF voltages, respectively. By using a stability diagram in  $a$ - $q$  space, the stability of ions of different mass-to-charge values can be evaluated at one time. A Mathieu stability diagram in  $a$ - $q$  space is shown in Figure 1.3.

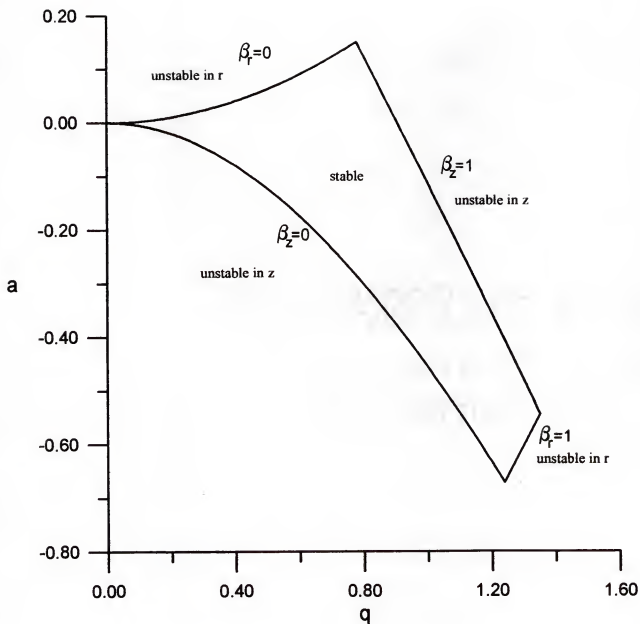


Figure 1.3

Mathieu stability diagram in  $a$ - $q$  space for a quadrupole ion trap mass spectrometer. The parameter  $a$  is proportional to the applied DC voltage, and the parameter  $q$  is proportional to the applied RF voltage.



As in a linear quadrupole, a mass spectrum is obtained by manipulating RF and DC voltages, in this case applied to the ring electrode, to direct ions of specific mass-to-charge values to strike a detector. Unlike a quadrupole, however, the processes of ionization and mass analysis typically occur sequentially in the same region of space. For electron ionization (EI), ions are formed by bombarding the sample molecules within the volume of the ion trap with electrons produced from a filament positioned behind one of the endcap electrodes; chemical ionization (CI) can also be performed in the ion trap simply by admitting a reagent gas and adjusting the timing sequence of operation to first form reagent ions which subsequently ionize sample molecules. During the ion formation period the RF voltage is held at a relatively low level to allow ions of a wide range of mass-to-charge values to be stored in the ion trap. The lowest  $m/z$  ion which is stable under any given conditions is referred to as the low-mass cutoff and is the  $m/z$  nearest the right side boundary of the stability diagram, i.e., at the  $\beta_z=1$  instability edge.

In the simplest scanning mode, the DC voltage applied to the ring is zero, and the endcap electrodes are held at ground potential. The mass analysis is accomplished by ramping the RF voltage from the initial low level, corresponding to the lowest mass of interest, to some higher voltage. As the voltage is increased, ions of successively higher mass-to-charge become unstable and are ejected from the ion trap, through holes in the endcap, to an external detector.

Computer control of the applied voltages is accomplished through a series of instructions assembled into what is referred to as a scan function. The scan

function is made up of a number of tables; each table indicates what voltages are to be applied and for what time. A basic scan function needs a table for each part of the experiment: ionization, ion containment, and mass analysis. The endcap electrodes are normally grounded, but an AC signal is applied to them during the mass analysis scan; this signal, which is  $180^\circ$  out of phase on the two endcaps, enhances the ion detection efficiency during the mass scan. A scan function for analysis of a sample using electron ionization is shown in Figure 1.4. The important traces in this scan function are the RF voltage, electron gate, and supplemental AC voltage. To perform more complex experiments, such as tandem mass spectrometry (to be discussed later in this chapter), one simply adds a table for each operation to be performed in the experiment.

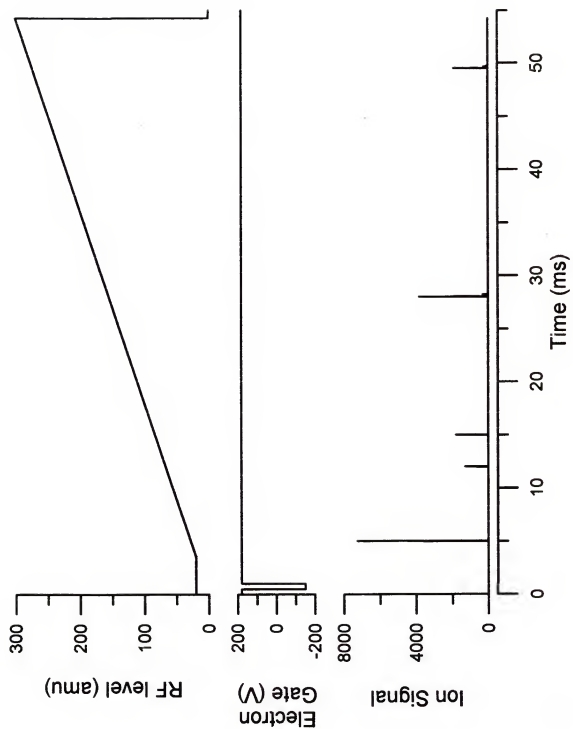
### Tandem Mass Spectrometry

Tandem mass spectrometry, or MS/MS, requires two stages of mass analysis. The first stage of mass analysis is used to choose ions of the particular mass-to-charge of interest. The selected ions are then dissociated, usually by collisions with a target gas. The second stage of mass analysis is then used to determine the mass spectrum of the dissociation products.

To perform MS/MS with a linear quadrupole device requires adding the ability to perform a second mass analysis, as well as adding a region to contain the ions during the dissociation step. These requirements necessitate adding hardware; second and third quadrupoles, with associated electronics and pumping, must be

Figure 1.4

Scan function for electron ionization operation of a quadrupole ion trap mass spectrometer. Ionization occurs during the first 1 ms of the scan function and mass analysis is performed during the RF ramp from approximately 4 ms to 53.5 ms.



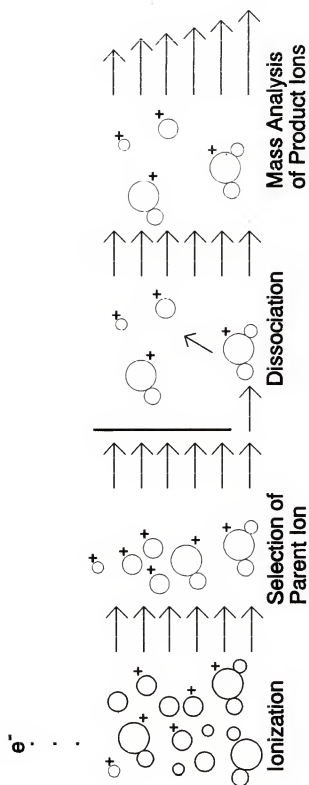
added to perform tandem mass spectrometry. Operation of a triple quadrupole mass spectrometer for the simplest MS/MS experiments involves ionization of the sample and scanning the third quadrupole, used for mass analysis of the dissociation product ions, in the same manner of operation of a simple quadrupole mass filter. The first quadrupole is used to select the mass-to-charge of interest, called the parent ion, by maintaining particular RF and DC voltages to allow ions of only one mass-to-charge value to pass through the filter. The second quadrupole, or collision cell, is a higher pressure region used to effect collision-induced dissociation of the parent ions. The second quadrupole is operated in RF-only mode; ions of many mass-to-charge values are stable in this region and can pass through to the third quadrupole for mass analysis. Figure 1.5 diagrams the general idea of tandem mass spectrometry.

In a quadrupole ion trap the MS/MS experiment is tandem-in-time in that all ion manipulation processes occur sequentially in the same region of space. Performing MS/MS in an ion trap consists of the same four basic steps as in a linear quadrupole: ionization of the sample, isolation of the mass-to-charge of interest, collision-induced dissociation of the isolated parent ions, and mass analysis of the resulting dissociation product ions. Ionization of the sample and mass analysis of the product ions are performed in the same manner as described above for obtaining a mass spectrum with an ion trap.

The isolation step is accomplished by applying a combination of RF and DC voltages to the ring electrode to make only a very narrow range of mass-to-charge values stable (generally this range is referred to as a single mass-to-charge,

**Figure 1.5**

**Concept of tandem mass spectrometry illustrating the steps of ionization of sample, selection of parent ion, dissociation of parent ion, and mass analysis of dissociation product ions.**



realizing that this is a single integer value). During the isolation step, ions of all but the selected mass-to-charge become unstable (i.e., fall outside the boundaries of the stability diagram) and are ejected from the ion trap either toward the ring or endcap electrodes.

In this work isolation is accomplished by one of two methods: apex isolation or two-step isolation. Both of these methods use the application of DC voltages to cause ions of all  $m/z$  values to become unstable except the one of interest. Apex isolation uses a negative DC pulse to move the ion of interest to the apex of the stability diagram (see Figure 1.3); at the apex, only one  $m/z$  will remain in a stable trajectory. This method removes ions of higher and lower  $m/z$  values in a single step using the  $\delta_x=0$  and  $\delta_x=1$  stability boundaries. Two-step isolation [24] removes ions of higher and lower  $m/z$  values in sequential steps using the  $\delta_x=0$  and  $\delta_x=1$  stability boundaries. Ions of higher mass-to-charge are removed using a positive DC pulse to move the  $m/z$  of interest to the  $\delta_x=0$  boundary; ion of lower  $m/z$  are then removed using a negative DC pulse after the RF is ramped to a point near the  $\delta_x=1$  boundary for the ion of interest. Two-step isolation has the advantage that the low and high mass isolations are independent and can be optimized separately, and this method has been shown to be more efficient in isolation than the apex method [24].

After isolation of the parent ion, a low amplitude supplemental AC voltage is applied to the endcap electrodes at the frequency of oscillation of the parent ion. This supplemental voltage is applied via a balun circuit so that the waveform on the



endcap electrodes is  $180^\circ$  out of phase. In this way the motion of the ions has an increased amplitude of oscillation, and the ions are "excited" through many collisions with the buffer gas. The excited ions undergo unimolecular dissociation, and the fragment ions are then analyzed by scanning the RF, as described previously, to obtain an MS/MS spectrum. One advantage of using an ion trap for tandem mass spectrometry is that the changes to go from MS to MS/MS are simply changes in the sequence of applied voltages; no hardware changes are necessary. This also allows for additional stages of dissociation and mass analysis as needed to perform MS/MS/MS or in general MS<sup>n</sup>.

### Thermospray Interface

The thermospray interface was developed to combine liquid chromatography and mass spectrometry by rapidly volatilizing the LC eluant as it passes through a resistively heated metal capillary [13]. The volatilized eluant is then directed into the ion source region of the mass spectrometer. Ions formed in the thermospray process are then extracted from the ion source into the mass analyzer. While the fundamentals of the thermospray process are not fully understood, at least two different mechanisms, direct ion evaporation of preformed ions from the droplets and chemical ionization of neutral sample molecules by the buffer ions, are believed to be responsible for ion formation [25,26,27]. Direct ion evaporation may occur for any species which exists as an ion in solution. Chemical ionization can produce sample ions through gas-phase reactions with reagent ions produced from

the ammonium acetate buffer if the conditions are favorable for gas-phase proton transfer; Figure 1.6 shows the ionization mechanisms believed to be responsible for formation of sample ions.

### Particle Beam Interface

Another approach to interfacing liquid chromatography with mass spectrometry was developed by Browner [28]; the particle beam interface (PBI) acts to separate species of lower volatility, typically the analytes, from species of higher volatility, such as the solvent. The PBI works by first nebulizing the LC eluant using a concentric flow of gas, usually helium. The nebulizer spray is directed into a heated chamber where solvent species are vaporized leaving largely desolvated particles of analyte and buffer species. The gas/particle stream is then directed into a momentum separator. In the momentum separator region, mechanical pumps are used to create regions of successively lower pressure which cause a supersonic expansion of the gas stream. A series of skimmers is used to separate the expanding gas from the higher momentum particles and direct the resulting particle beam into the mass spectrometer. Unlike thermospray, the PBI does not act to ionize the sample; the PBI merely transports the neutral analyte into the mass spectrometer ion source where ionization occurs. Some solvent is also transported into the mass spectrometer; this solvent can be used as a reagent gas for chemical ionization [29]. This form of ionization has been shown to be particularly useful in ion trap mass

### Reagent Ion Formation



### Chemical Ionization Reactions

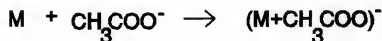
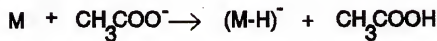
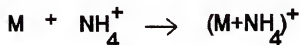


Figure 1.6

Ionization mechanisms for thermospray interface operating in filament-off mode.

spectrometry where EI and CI can be performed using the same hardware; thus, information on structure and molecular weight can be gained by alternating between EI and CI during acquisition [29].

### Overview of dissertation

This dissertation presents studies to examine the use of electrochemistry/mass spectrometry for studying the degradation or metabolism of environmental contaminants and studies to characterize rapid removal of the RF to effect ejection/detection of ions stored in a quadrupole ion trap. Chapter 2 will describe EC/MS studies of N,N-dimethyl aniline and benzdine performed using TSP/MS. EC/MS was also performed using PB/MS; these results for aniline, anisidine, and benzdine will be discussed in Chapter 3. Chapter 4 introduces a different operational mode for use with the ion trap. This method shows improved signal versus the standard operating method; the utility of this method, along with implications for its use with EC/MS, will be discussed. The final chapter of this dissertation, Chapter 5, contains conclusions and suggestions for future studies to the work presented herein.

## CHAPTER 2

### EXAMINING THE OXIDATION OF AROMATIC AMINES BY ON-LINE ELECTROCHEMISTRY/THERMOSPRAY/MASS SPECTROMETRY

#### Introduction

The study of the pathways and ultimate products in the oxidation of environmental contaminants is a significant concern for monitoring applications interested in determining the potential hazard a particular analyte may pose. Electrochemistry can provide valuable insight into oxidation products [4], but the long reaction times associated with bulk electrolysis may affect the diagnosis of a potential toxin because some information may be lost from short-lived intermediates which do not survive long enough for analysis. The use of on-line electrochemistry provides a more suitable platform to analyze potentially carcinogenic samples [30].

In this chapter, the use of electrochemistry/thermospray/mass spectrometry (EC/TSP/MS) is presented and discussed for analysis of benzidine and N,N-dimethyl aniline (DMA). These two compounds, while in the same general class, exhibit significantly different behavior in EC/TSP/MS experiments. Mass spectrometric hydrodynamic voltammograms (MSHV) of each show, as does off-line cyclic voltammetry, oxidations occurring at similar potentials, but the MSHV's indicate different results of the oxidation. The results for DMA obtained here also show

some marked differences from results reported in previous work by Hambitzer and Heitbaum [14].

### Electrochemical Equipment

All electrochemical experiments were performed using an EG&G Princeton Applied Research model 173 potentiostat and model 175 universal programmer. The potentiostat was used alone in single potential experiments and in conjunction with the programmer for multipotential experiments, such as cyclic voltammetry and pulsed-potential experiments. An X-Y recorder was used to record the data for off-line cyclic voltammetry.

The flow-through cell used in all on-line EC/MS was an ESA model 5020 guard cell; a diagram of the cell is shown in Figure 2.1 [31]. The cell has a paladium reference and a paladium counter electrode. The working electrode is constructed from reticulated vitreous carbon. The volume of the cell is approximately 5  $\mu$ L, according to the manufacturer. The cell is constructed of stainless steel and designed to withstand backpressures of up to 6000 psi. The cell is connected to the system by the use of 1/16" stainless steel HPLC tubing with Valco fittings.

### Mass Spectrometer

A Finnigan TSQ45 triple quadrupole mass spectrometer was used for all EC/TSP/MS experiments. The TSQ45 system is a standard, commercially available system equipped with a Vestec thermospray LC/MS interface. The instrument is

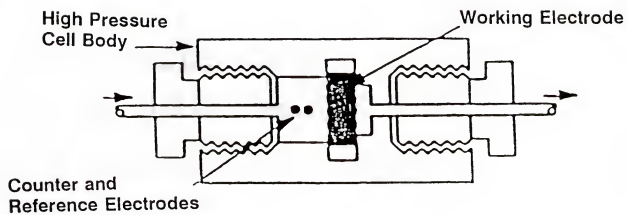


Figure 2.1

Diagram of ESA model 5020 electrochemical cell.

tuned and calibrated using the tuning compound perfluorotributyl amine (PFTBA) while operating with an electron ionization source in place. The thermospray ion source uses an additional 300 L/min mechanical pump in combination with a liquid nitrogen cold trap to remove the excess vapor delivered to the source. The thermospray ion source was operated in our work in the filament-off mode; that is only ions produced by the thermospray process itself were available for analysis. A sample cone with a 500  $\mu\text{m}$  aperture is used to reduce the gas load entering the mass analyzer region of the instrument. There are many interfering ions produced by the thermospray process below  $m/z$  150; to avoid these interferences, the quadrupole was scanned over the mass range from 150 u to 450 u in these experiments. Typical operating conditions for the thermospray interface were tip temperature of 220°C and source temperature of 290°C when using a 0.1 M ammonium acetate solvent flowing at 1.0 mL/min.

### Mass Spectrometric Hydrodynamic Voltammograms

On-line electrochemical experiments are preceded by off-line cyclic voltammetry to examine the electrochemical behavior of the analytes, specifically to determine potentials at which oxidation occurs for the analytes. The principle of cyclic voltammetry can be modeled on-line by creating a mass spectrometric hydrodynamic voltammogram [31]. A mass spectrometric hydrodynamic voltammogram results from a series of EC/MS experiments in which the electrochemical potential is varied in a systematic manner to obtain mass-intensity



data at multiple points in the potential range covered by the cyclic voltammogram. Although the mass spectrometric hydrodynamic voltammogram cannot be reversed, the general shape of the mass spectrometric hydrodynamic voltammogram follows that of the cyclic voltammogram. The mass spectrometric hydrodynamic voltammogram has the advantage that multiple  $m/z$  ions can be observed to show decreases in the analyte and increases in product species.

EC/TSP/MS experiments were accomplished by flow-injection of 10  $\mu\text{L}$  of sample solution into 0.1 M ammonium acetate buffer solution at a flow rate of 1.0 mL/min into the EC cell. The eluant from the EC cell was then directed into the thermospray interface. Mass analysis was performed by scanning the first quadrupole and operating the second and third quadrupoles in RF-only mode. The potential applied to the electrochemical cell was varied to produce a mass spectrometric hydrodynamic voltammogram. The potential on the EC cell was changed manually between sets of triplicate injections to vary the potential from 0 V to +1 V vs Pd incrementing the potential in 100 mV steps. A diagram of the EC/TSP/MS system is shown in Figure 2.2.

#### Off-line Electrochemistry

Prior to performing electrochemistry on-line, the compounds of interest were examined via off-line cyclic voltammetry. Cyclic voltammetry was performed in the flow cell under stop-flow conditions using solutions 1 mM in the compounds of interest. The electrochemical potential was scanned from 0 V to +1 V and back

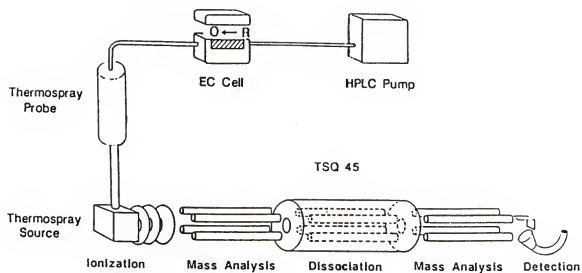


Figure 2.2

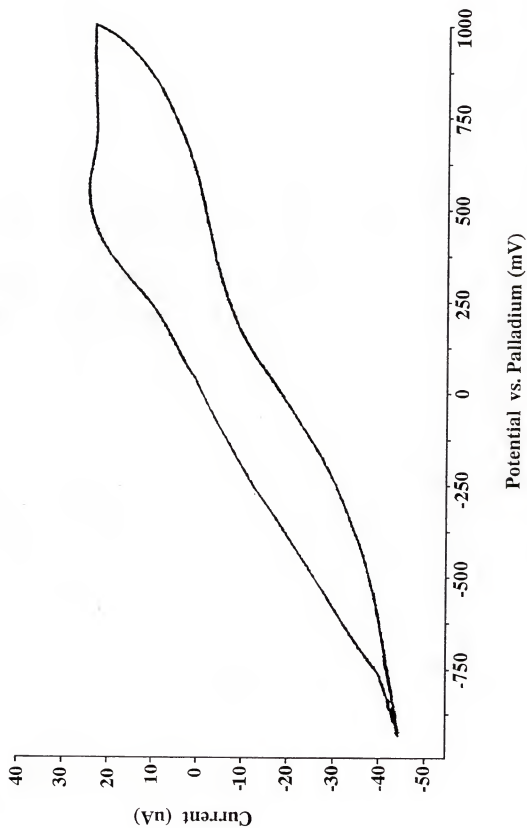
Diagram of the electrochemistry/thermospray/mass spectrometry system used [17].

to 0 V vs Pd at a rate of 5 mV/s; the CV for benzidine obtained in this manner is shown in Figure 2.3. The oxidation peak appears at approximately +600 mV vs Pd. The CV obtained in the flow cell has a weak oxidation peak due to the electrode configuration and characteristics. Other CVs obtained in this manner show similarly weak responses; all of the aromatic amines studied showed an oxidation peak around +600 mV vs Pd.

Electrochemistry was performed in conjunction with liquid chromatography (EC/LC) using a fixed-wavelength UV detector. A 5  $\mu$ L aliquot of a 1 mM benzidine solution in 0.01 M ammonium acetate was injected into the solvent flow at 0.25 mL/min. The sample passed through the EC cell which was poised at an appropriate potential (0 or +600 mV vs Pd). The effluent from the EC cell was directed onto a 15 cm x 2 mm i.d. C-18 (octadecyl silane) column. The detector output was monitored using a chart recorder with paper speed of 2 cm/min. The results were disappointing in that only one peak was observed, corresponding to the retention time of the benzidine, even under conditions for oxidation (i.e., the electrode poised at +600 mV vs Pd). The peak area decreased when a potential of +600 mV was applied to the EC cell, but no other peaks appeared. Gradient conditions were also used in an attempt to elute strongly retained species, but still only one peak was observed. Any products which are being formed may be adsorbed to the electrode material or to the column packing and thus not be detected. The increase in backpressures associated with the electrochemical cell indicate that some

Figure 2.3

Cyclic voltammogram for benzidine obtained under stop-flow conditions in the ESA model 5020 electrochemical cell; a scan rate of 5 mV/s was used for collection of these data.



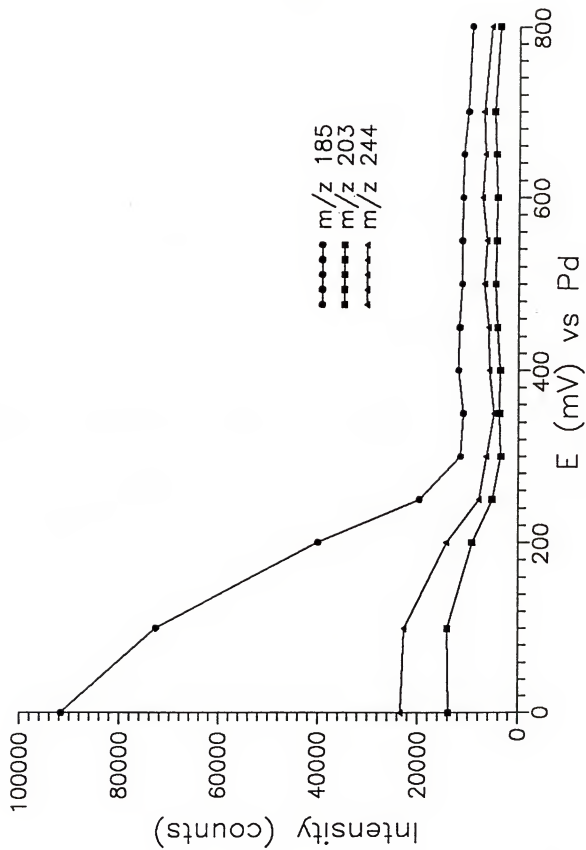
material is being deposited on the electrode and clogging the pores; this suggests that the losses of products may in fact be due to the adsorption processes discussed above.

### On-line Electrochemistry

EC/TSP/MS was first performed on benzidine. The resulting mass spectrometric hydrodynamic voltammogram (MSHV) for benzidine, shown in Figure 2.4, shows significant losses of the protonated molecule and other molecular adduct ions but no product ions increasing. These results are similar to those seen in the EC/LC experiments where a decrease in the benzidine peak area was observed, but no product peaks appeared. The large decrease in peak area for the protonated benzidine and adduct ions indicates significant conversion of the benzidine at the applied electrochemical potentials; however, the absence of any ions corresponding to products gives no insight into what these products may be. Figure 2.5 shows the mass spectra of benzidine at applied potentials of 0 and +500 mV vs Pd. Notice that the major ions in each spectrum are the same,  $m/z$ 's 185, 203, and 244, but the relative intensities are changed as the protonated molecule ( $m/z$  185) decreases to a larger extent. The species formed upon the oxidation of benzidine must, therefore, not be making it to the ion source of the mass spectrometer (or not forming ions to mass analyze). The products could be adsorbing to the electrode material upon being oxidized and thus be removed from the sample stream. Or the products may not be amenable to the thermospray process and simply do not form any ions to be

Figure 2.4

Mass spectrometric hydrodynamic voltammogram of benzidine obtained by electrochemistry/thermospray/mass spectrometry. Shown are mass chromatograms for the  $(M+H)^+$ ,  $(M+NH_4)^+$ , and  $(M+HOAc)^+$  ion at  $m/z$  185, 203, and 244, respectively.





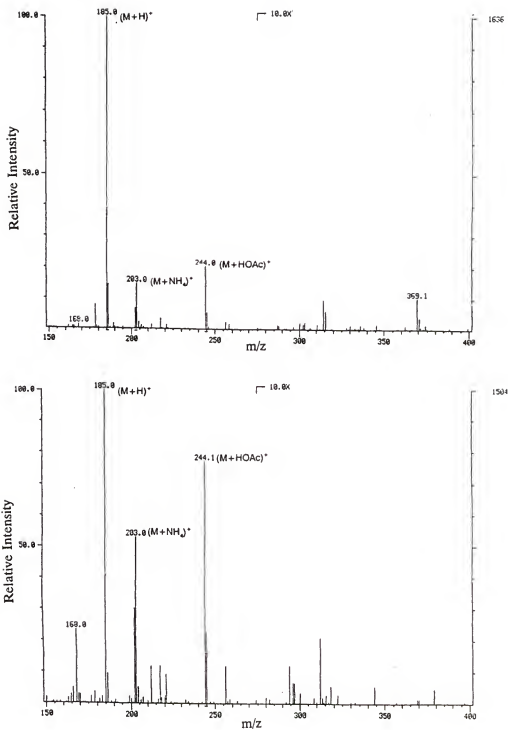


Figure 2.5

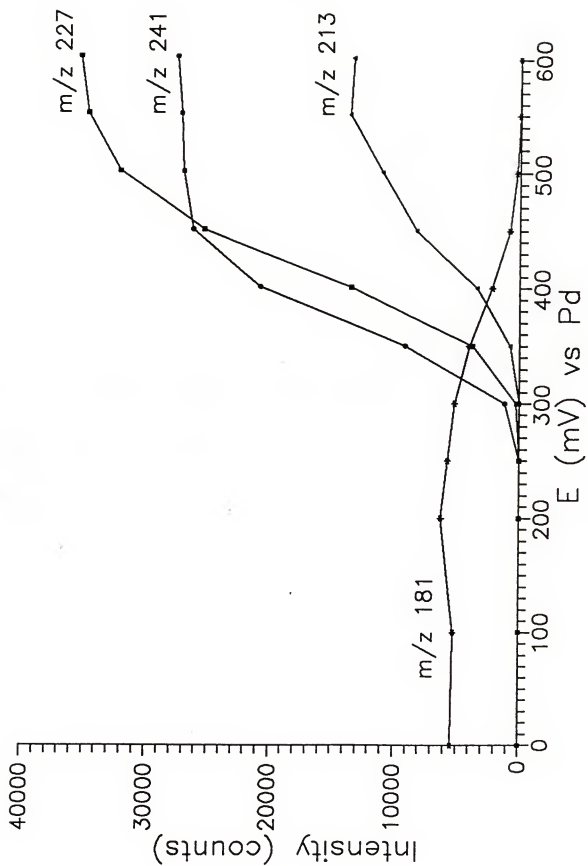
Mass spectra of benzidine taken at electrochemical potentials of a) 0 mV and b) 500 mV vs Pd.

mass analyzed. The differences in the EC using TSP from the PB/MS experiments (which will be discussed in the next chapter) could be associated with the differences in flow rates used which affect the contact time between the sample and the electrode (which relates to the flow rate used) and with the different solvent compositions used (no organic component in the TSP experiments).

EC/TSP/MS was also performed on *N,N*-dimethyl aniline. The MSHV for *N,N*-dimethyl aniline (DMA) obtained by EC/TSP/MS is shown in Figure 2.6. An acetic acid adduct ion at  $m/z$  181 was used to monitor the DMA due to high background in the molecular ion region of the spectrum ( $m/z$  120-150). Figure 2.7 shows the mass spectra obtained for dimethyl aniline at applied potentials of 0 and +600 mV vs Pd. The product ion at  $m/z$  241, presumably due to the formation of *N,N,N',N'*-tetramethylbenzidine (TMB) through dimerization of DMA [14], begins to appear at a potential of +250 mV vs Pd. The ion at  $m/z$  227 has previously been attributed to a fragmentation of  $(\text{TMB}+\text{H})^+$  [14]; however, the mass intensity data for  $m/z$  227 does not parallel that for  $m/z$  241 as one would expect for a fragment ion. This exemplifies the advantage of obtaining a complete MSHV through which all species of interest can be observed at all potentials examined. The intensity for the  $m/z$  213 species also does not parallel either of the other two ion intensities, suggesting that this may be a different oxidation product as well. The number of different ions appearing in the MSHV suggest that several products are being formed, though none of these decreases at higher potentials as one might expect.

Figure 2.6

Mass spectrometric hydrodynamic voltammogram of N,N-dimethyl aniline obtained by electrochemistry/thermospray/mass spectrometry. Shown are mass chromatograms for the  $(M+HOAc)^+$  ion 181 and product ions at  $m/z$ 's 213, 227, and 241.



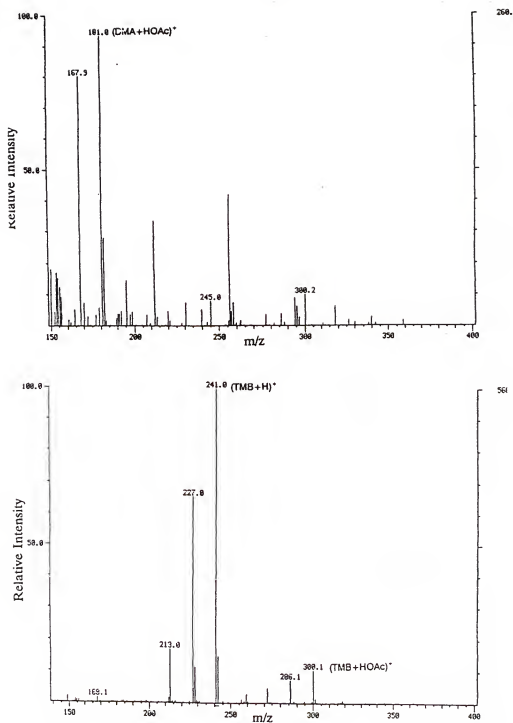


Figure 2.7

Mass spectra of N,N-dimethyl aniline taken at electrochemical potentials of a) 0 mV and b) 600 mV vs Pd.

Tandem mass spectrometry might be useful in examining possible structures of these various product species and confirming electrooxidation pathways.

### Conclusions

The electrochemistry/thermospray/mass spectrometry system used provided opportunity to examine the oxidation of benzidine and dimethyl aniline (DMA) using an aqueous solvent system. The results obtained for benzidine indicate that while a significant decrease in the signal for benzidine is observed, no electrochemical products are seen in the mass spectra. The experiments with electrochemistry/mass spectrometry of dimethyl aniline, however, yielded interesting results. The same product ions reported by other researchers [8] were also observed in our work, but there is not correlation of some of these species with the identifications made by Hambitzer and Heitbaum. The advantage of a mass spectrometric hydrodynamic voltammogram is apparent in determining in this work that ions observed at  $m/z$ 's 213 and 227 are not simply fragment ions of the main product of the oxidation of DMA, but are indeed other products being formed.

# CHAPTER 3

## PARTICLE BEAM/ION TRAP MASS SPECTROMETRY FOR THE INVESTIGATION OF AROMATIC AMINES USING ON-LINE ELECTROCHEMISTRY

### Introduction

The particle beam interface (PBI) offers another method to interface liquid phase chemistry and mass spectrometry. The PBI has significantly different optimum operating conditions than does thermospray: organic or mixed organic/aqueous solvent systems are preferred, and flow rates of 0.5 mL/min or less are most commonly used. In addition, because the PBI merely transports the neutral analytes into the mass spectrometer where they are vaporized upon striking a heated target (before ionization by electron or chemical ionization), analytes must not be thermally labile or involatile. These differences would limit PBI alone but help to extend the range of experiments possible when used as a companion technique to thermospray.

The quadrupole ion trap mass spectrometer (QITMS) is a versatile instrument which can be used to perform simple mass spectrometric experiments or complex tandem mass spectrometric (MS/MS) work by changing the sequence of applied voltages. The ion trap has the advantage that no additional hardware is needed to advance from MS/MS to MS/MS/MS and beyond. Additionally, the ion trap has the capability to operate in various ionization modes (for example, electron

ionization or chemical ionization) without hardware changes. These capabilities make the ion trap well suited for use in electrochemistry/mass spectrometry work.

### Particle Beam Interface

The particle beam interface (PBI) used in these studies is a Finnigan MAT prototype interface designed with a third stage of momentum separation specifically to reduce the amount of solvent vapor that is transmitted through the device and into the ion trap. A diagram of the interface is shown in Figure 3.1. The PBI uses a glass, concentric nebulizer with helium as the nebulizing gas. The aerosol is carried into a heated desolvation chamber; the resulting vapor and particles travel into the momentum separator. The desolvation chamber was modified in our laboratory to allow control of the pressure in the chamber by addition of helium through a needle valve; the pressure in the chamber is monitored by a pressure gauge. Additional helium in the desolvation chamber allows for more efficient heat transfer from the walls of the chamber to the aerosol droplets. The amount of helium used for nebulization also affects the intensity of ions ultimately measured in the ion trap. Optimization of the pressure of the nebulizer helium is an important process in optimization of the ion signal. Figure 3.2 shows the effect of nebulizer helium pressure on the response of anisidine. As the data show, the intensity of the molecular ion of anisidine ( $m/z$  123) optimizes over a narrow range of nebulizer helium pressure around 15 psi. Response for other amines shows similar trends to



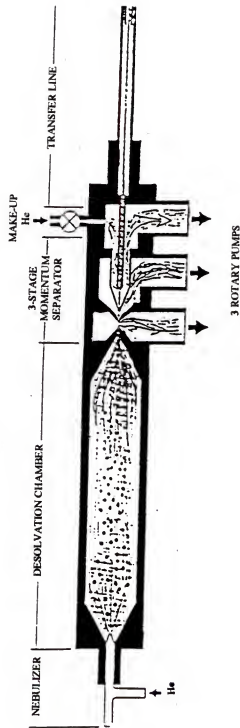


Figure 3.1

Diagram of a particle beam interface. The four regions of the interface (from left to right) are the nebulizer, desolvation chamber, momentum separator, and transfer line.

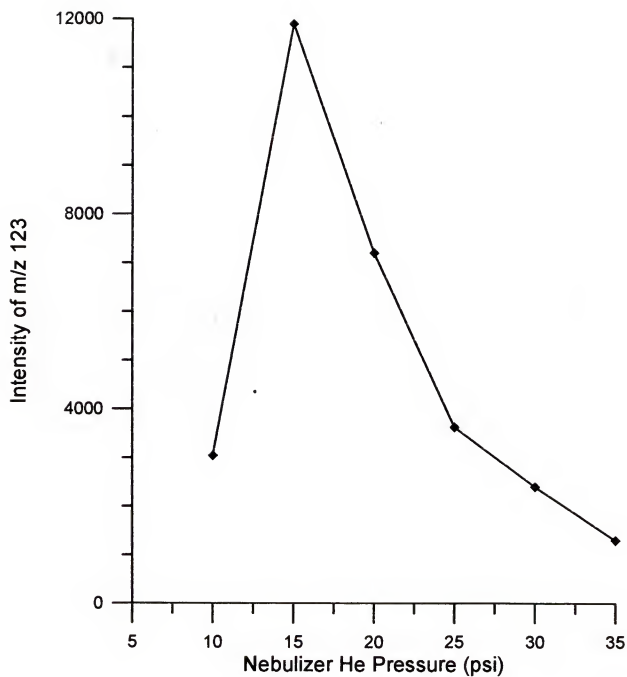


Figure 3.2

Optimization of nebulizer helium pressure for the PBI; plotted is the response of anisidine vs the helium pressure.

that of anisidine; it was found that optimization with one of the compounds in this class provides good operating conditions for the others as well.

### Mass Spectrometers

Two quadrupole ion trap systems were used in electrochemistry/particle beam/mass spectrometry experiments: a Finnigan ITMS and an instrument constructed in our laboratory based upon a Finnigan ITS40. The ITMS is a commercial research-grade quadrupole ion trap mass spectrometer. The voltages applied to the electrodes are controlled by computer. The ITMS is normally operated with helium added into the vacuum chamber to an uncorrected pressure of  $1.1 \times 10^{-4}$  torr as measured by an ion gauge. Electron ionization is effected by gating electrons from a thorium-iridium filament into the ion trap. Tuning of the mass spectrometer and mass calibration are performed using the tuning compound PFTBA. Ion Catcher Mass Spectrometer (ICMS) software developed in our laboratory [32] is used to operate the ITMS and collect mass spectral data; the ICMS software has additional capabilities, which will be discussed in more detail later, that facilitate some of the experiments performed.

The vacuum chamber of the ITMS is designed with a vacuum lock which allows the insertion and removal of a solids probe or GC transfer line without venting the system. This probe lock is used for the particle beam interface as well; the probe shaft of the PBI is inserted through the probe lock so that the particle beam exits the interface and strikes the hyperbolic surface of the entrance endcap

of the ion trap. The distance from the end of the PBI shaft to the entrance hole in the endcap is significant in determining the pressure in the ion trap. When the shaft is touching the endcap the peak shapes in the mass spectrum are distorted; the presumption is that the pressure in the ion trap is higher than the indicated chamber pressure due to the excess helium and solvent vapor flowing into the trap from the PBI. When the shaft is pulled back about 1/4" from the endcap, the peak shapes return to normal and sensitivity improves. The open space between the end of the shaft and the endcap allows for the gas from the PBI to disperse into the chamber. Positioning the end of the shaft at distances more than 1/4" from the endcap appears to make little difference in the ion intensities or peak shapes.

For efficient vaporization of the particle beam, an entrance endcap was modified so it could be heated independently of the ITMS; two holes were drilled into the base of the endcap into each of which a cartridge heater is inserted. The cartridge heaters are controlled by an Omega temperature controller using a thermocouple to monitor the temperature of the endcap. After modification, the endcap was able to be heated up to 300°C. The target temperature for optimum ion signal was optimized using anisidine as a test compound. The temperature of the endcap directly affects the amount of neutral analyte vaporized from the particle beam. If the temperature is too low the sample will deposit on the endcap and slowly burn off resulting in reduced sensitivity and poor peak shape; however, if the endcap temperature is too high, thermal degradation of the sample may occur during the vaporization process. Figure 3.3 shows a plot of endcap temperature versus  $m/z$

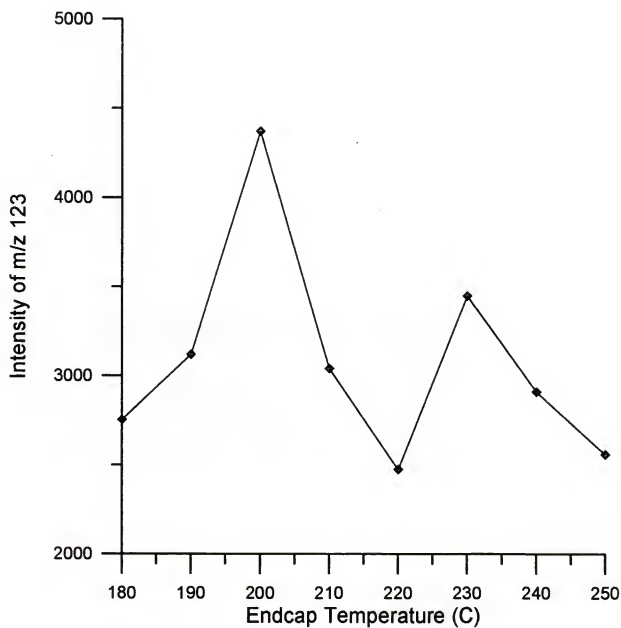


Figure 3.3

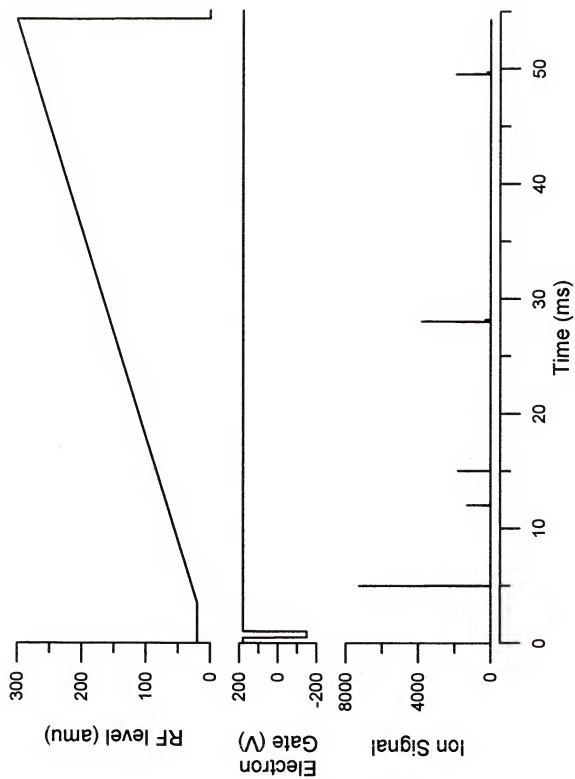
Optimization of the endcap (target) temperature for PBI/MS operation; plotted is the response of anisidine vs endcap temperature.

123 intensity. The data indicate that the endcap should be operated near 200°C for optimum molecular ion signal.

An electron ionization scan function consists of several basic steps including triggering of the instrument, ionization of the sample, a cooling period, and the analytical scan. Generally, the RF level is held constant until the mass analysis scan; the mass range of the analysis is determined in this case by the low mass cutoff during ionization and the high mass point of the analytical scan. When operating with a particle beam interface the low mass cutoff during ionization may allow for the ionization of unwanted solvent as well as the sample. The RF level can be manipulated, either during or after the ionization step, to remove these solvent ions prior to the analytical scan; however, raising the RF level during ionization is often detrimental to overall ionization efficiency. A scan function used for electron ionization during EC/PBI/MS analyses appears in Figure 3.4.

During electron ionization, the solvent ions are undesirable contributors to space-charge effects in the ion trap; however, these same solvent ions can be utilized for chemical ionization of the sample [33]. Chemical ionization is accomplished by ionizing the sample and solvent using an electron beam, then mass isolating the solvent ions of interest and allowing time for proton transfer reactions to occur between these solvent ions and neutral analyte molecules in the ion trap. Chemical ionization is a softer ionization technique which generally produces simpler spectra than electron ionization because chemical ionization causes a lower degree of fragmentation. The ions produced during the reaction time then undergo mass

Figure 3.4      Scan function used for EC/PBI/ITMS experiments. Ionization occurs from 1-2 ms, and mass analysis is performed during the RF ramp from 4-51 ms.





analysis via standard mass-selective instability scanning. A scan function used for methanol chemical ionization is shown in Figure 3.5. The important regions in the scan function include ionization of reagent gas by EI (1-5 ms), isolation of the reagent ion via apex isolation (5-8 ms), reaction time for ionization of sample through proton transfer from reagent ions (8-18 ms), and mass analysis after removing excess reagent ions by raising the RF (18-69 ms).

The Finnigan ITS40 is designed as a gas chromatography/mass spectrometry system with the ion trap contained in a relatively small vacuum chamber. For our work, the ion trap was removed from the commercial vacuum chamber and placed in a larger, custom-built chamber. The new chamber has a center wall which can be used to separate the chamber into two differentially pumped regions: one for an ion source and one for the analyzer. The chamber was designed to accommodate two types of ion sources: a standard Finnigan 4500 EI/CI ion source and a Finnigan electrospray ionization source. The ion trap could be operated using one of these external ion sources or using standard internal ionization. The ion trap is oriented in the chamber such that ions from the ion source are injected axially, that is through the holes in one endcap. Helium, necessary for efficient trapping, is plumbed directly into the ion trap through 1/8" stainless steel tubing. A diagram of the modified ITS40 system with the EI/CI source installed is shown in Figure 3.6.

Along with the hardware modifications made to the ITS40 system, new software was also developed in our laboratory [34]. The new software allows for customization of scan functions and for control of additional parameters needed for

**Figure 3.5** Scan function used for methanol chemical ionization during EC/PBI/ITMS experiments.

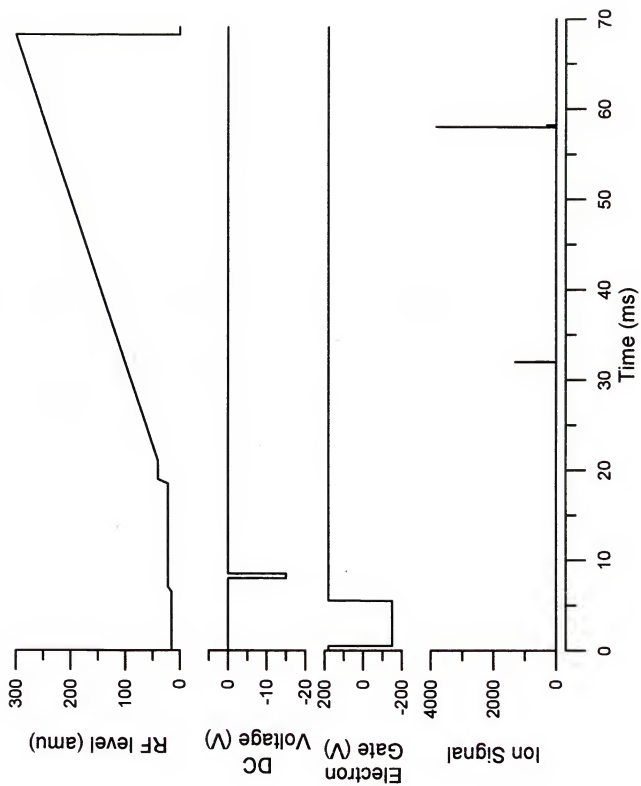
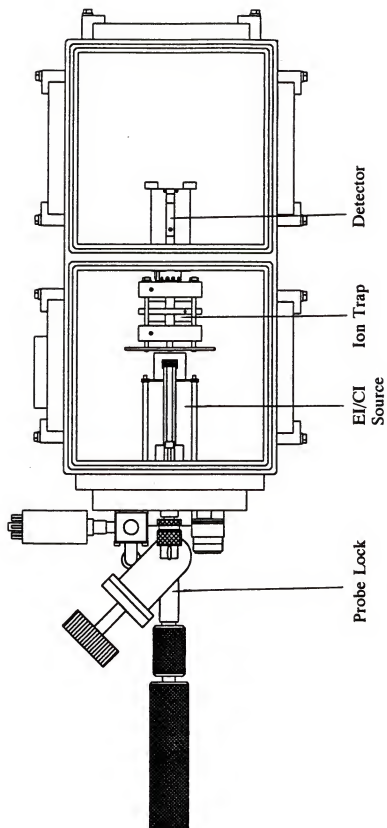


Figure 3.6

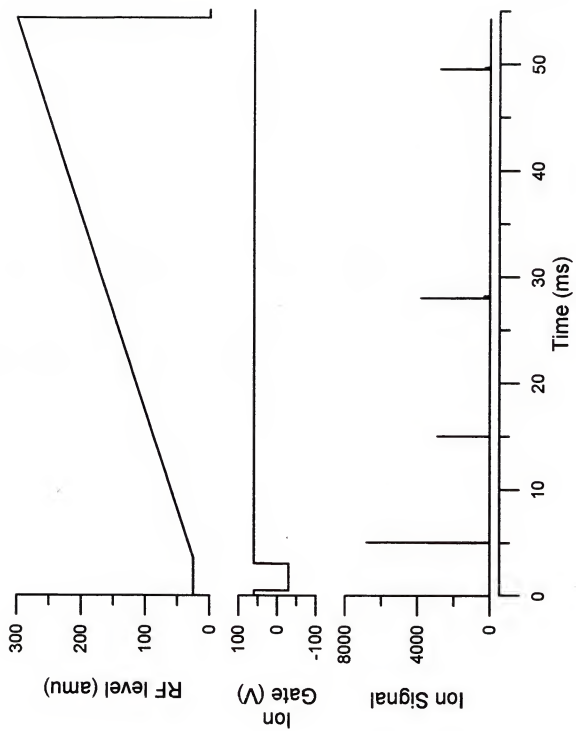
Diagram of the ion trap system constructed in our laboratory based around a Finnigan ITS40 ion trap mass spectrometer.



ion injection and ion isolation. The scan functions used with the ITS40 system have three basic areas: ion injection, ion manipulation, and mass analysis. Figure 3.7 shows an example of a scan function used for PB/EC/ITS40 experiments. Ion injection is accomplished by pulsing a gate electrode, held "closed" at +60 V, to -30 V to allow ions formed in the ion source to pass through to the ion trap; the ion injection time was 1 ms to 20 ms depending on the nature of the experiment and the sample. Ion manipulation processes, such as ion isolation, and mass analysis are performed as on the ITMS.

The use of an external ion source requires that the ions be transported from the ion source where they are created to the ion trap where mass analysis will occur. The ion sources that were used in this work were designed with a system of electrostatic lenses which are used to extract ions from the source and focus the ion beam and direct it toward the mass analyzer. The original intent for these sources was for use with quadrupole mass analyzers which the ions would pass through. If an ion trap is used the ion beam must be stopped before passing through the analyzer. In either instance, the analyzer must be at a negative potential relative to the grounded ion source for positive ions to move from the source to the analyzer; this potential difference determines the ion energy. For injection of ions into an ion trap the ion energy must be high enough to allow the ions to penetrate the potential fields of the ion trap but not so high that the ions simply traverse the ion trap and exit through the other side. The ion signal was found to optimize at ion energies between 2 and 4 eV; the exact optimum did vary within this range as tuning

**Figure 3.7** Scan function used for EC/PBI/ITS40 experiments.





parameters were changed. The ion energy was adjusted manually to maximize ion signal before each set of experiments.

Helium buffer gas plays a very important role in reducing the energy of the injected ions so they can be trapped. In the modified chamber design, helium is plumbed directly into the ion trap via 1/8" stainless steel tubing. The pressure of helium in the ion trap is approximately a factor of ten higher than the pressure in the chamber surrounding the ion trap due to the limited conductance of the ion trap [35]. The chamber pressure is monitored by an ion gauge mounted on a side flange of the chamber. The optimum ion signal is obtained when helium is added to give an uncorrected ion gauge reading of  $1 \times 10^{-5}$  torr.

The magnitude of the RF voltage applied to the ring during ion injection also affects ion signal. Figure 3.8 shows the variation of ion intensity for the six major ions of PFTBA as the RF level during ion injection is changed. The data indicate that four of the six ion optimize at an RF level of 25 u during ion injection; this is the level that is typically used in EC/PB/TTS40 experiments. It should also be noted that the relative intensities of the ions change significantly as the RF level is varied; while  $m/z$  69 remains the ion of highest intensity, its relative intensity increases significantly when the RF level is changed from 20 to 30 u. Although all of the ions followed in this experiment are fragment ions,  $m/z$  69 ( $\text{CF}_3^+$ ) has the most possible pathways for formation; therefore, when the ion energies are increased by raising the RF level more fragmentation occurs which leads to the production of a relatively

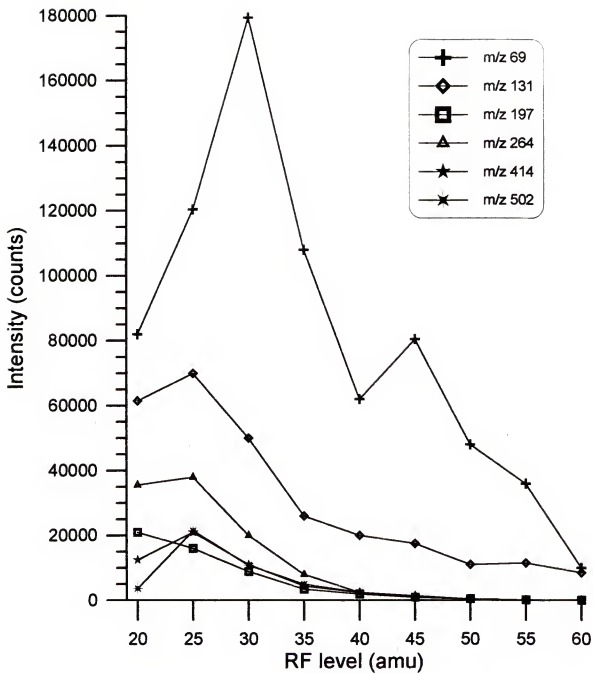


Figure 3.8

Optimization of RF level during ion injection period on modified ITS40 system. Plotted are the ion intensities for m/z's 69, 131, 197, 264, 414, and 502 from PFTBA vs the low mass cutoff.

larger percentage of  $\text{CF}_3^+$  than that which is produced by the electron ionization process.

A more detailed examination of this phenomenon was undertaken when software capabilities were made available through efforts in our laboratory [34]; the results are consistent with those of the earlier study. Figure 3.9 shows the ion intensities plotted versus the RF level expressed u. Figure 3.10 shows these same intensity data plotted versus the Mathieu parameter  $q$ . The ion intensities of all but  $m/z$  69 maximize at an Rf level of approximately 25 u. Again, the lower mass fragment ions, particularly the  $\text{CF}_3^+$  ion at  $m/z$  69, have broad peaks at significantly higher RF levels possibly indicating fragmentation resulting from the higher energy ions at higher RF voltages. The two peaks in the plot for  $m/z$  414 support the theory that two processes are occurring; one maximum corresponding to the optimum trapping of  $m/z$  414 ions produced in the ion source, the other to trapping of  $m/z$  414 ions produced by fragmentation of higher  $m/z$  ions as they enter the ion trap.

EC/PB/ITMS experiments were performed using infusion injection of the sample solution through the EC cell and into the PBI for introduction into the ion trap. An Isco syringe pump was filled with the sample solution. A diagram of the EC/PB/ITMS system is shown in Figure 3.11. The solution was flowed into the EC cell at flow rates ranging from 0.05 mL/min to 1.0 mL/min; typically, a flow rate of 0.10 mL/min was used in EC/ITMS experiments. Ionization of the sample was accomplished by electron ionization in most cases, although solvent chemical ionization [33] was used in some instances. The use of chemical ionization generally

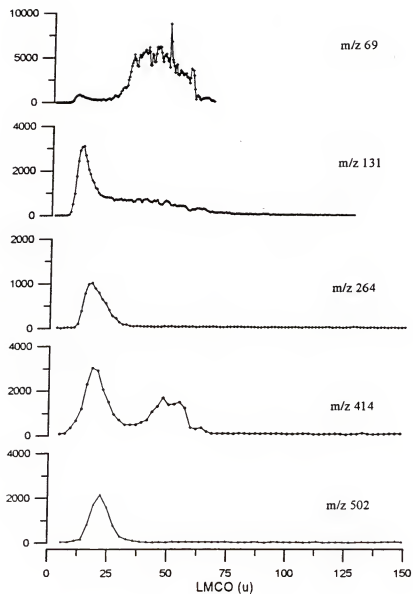


Figure 3.9

Optimization of RF level during ion injection period on modified ITS40 system. Plotted are the ion intensities for m/z's 69, 131, 264, 414, and 502 from PFTBA vs the low mass cutoff.

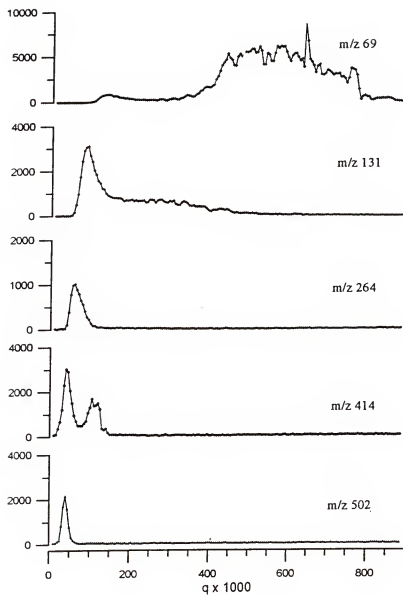


Figure 3.10

Optimization of RF level during ion injection period on modified ITS40 system. Plotted are the ion intensities for  $m/z$ 's 69, 131, 264, 414, and 502 from PFTBA vs the  $q$  of the particular  $m/z$  ion.

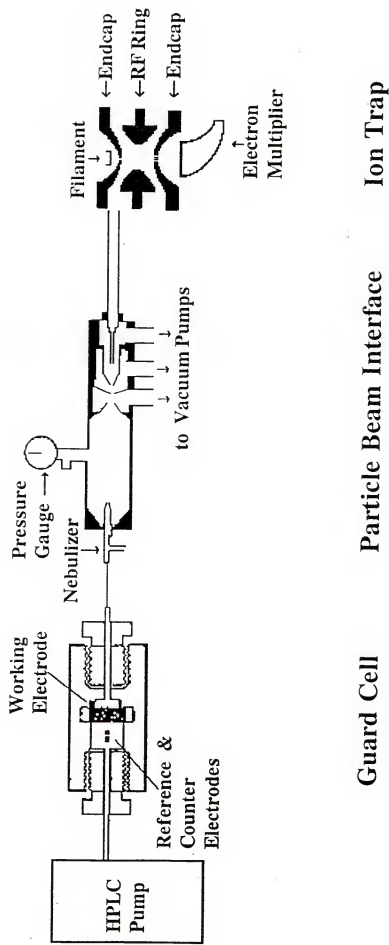


Figure 3.11 Diagram of the electrochemistry/particle beam interface/ion trap mass spectrometer system

allows the ion signal to be concentrated in one  $m/z$  thus increasing the sensitivity. The ITMS was operated in standard mass-selective instability scanning mode using axial modulation.

To perform an EC/MS experiment, the EC electrode was poised at 0 V for 30 s with the mass spectrometer scanning. The electrode was then pulsed to the desired potential to perform oxidation of the analyte and returned to 0 V after 60 s. In this way, the molecular ion signal of the analyte decreases when the electrode is pulsed. For EC/MS/MS experiments, the potential of the electrode was held at the positive potential which had through EC/MS produced an ion not in the analyte's original mass spectrum; the "new" ion was then isolated and dissociated to yield product ions which could be used to deduce the structure of the electrochemical product.

EC/PB/ITS40 experiments were performed using the same three-stage PBI as used for the EC/PB/ITMS experiments; however, an HP 1090 liquid chromatography system was used for sample introduction. The use of the chromatography system facilitated the production of mass spectrometric hydrodynamic voltammograms in the same manner as those created using the EC/TSP/TSQ system.

### Electrochemistry/Particle Beam/ITMS

Initial studies were undertaken to characterize the EC/PBI/ITMS system using electron ionization of benzidine. The first parameter examined was effect of

flow rate on the electrochemical conversion efficiency. A plot of electrochemical conversion efficiency, measured as the decrease in intensity of the molecular ion of benzidine, versus the flow rate through the EC cell is shown in Figure 3.12. The data points show the decrease in the benzidine signal, expressed as a percentage, at the steady-state level achieved during a 100 s potential pulse. The data indicate that the electrochemical conversion efficiency of the cell is >65% at flow rates of 0.10 mL/min or less but decreases dramatically at higher flow rates, dropping below 30% at a flow rate of 1.0 mL/min. These experiments demonstrate that using flow rates below 0.25 mL/min is necessary to achieve conversions of at least 50%.

Ion intensities during and following a potential pulse illustrating the results of electrochemistry/particle beam/mass spectrometry (EC/PBI/MS) for benzidine are shown in Figure 3.13. These traces are commonly referred to as chromatograms even though no chromatographic separation is being performed. The top trace in the figure is the mass chromatogram for the molecular ion of benzidine ( $m/z$  184,  $M^+$ ). The middle is the mass chromatogram of the oxidation product at  $m/z$  305. The bottom trace shows the potential applied to the EC cell. The decrease in the benzidine molecular ion signal begins approximately 50 s after initiation of the potential pulse to the EC electrode. The delay in the onset of the decrease in the benzidine signal is due to the dead volume between the EC cell and the PBI. Occurring simultaneously with the decrease in benzidine signal is an increase in signal at  $m/z$  305; this ion was not present in spectra of benzidine taken when the EC potential is zero and must then correspond to an electrochemically generated product



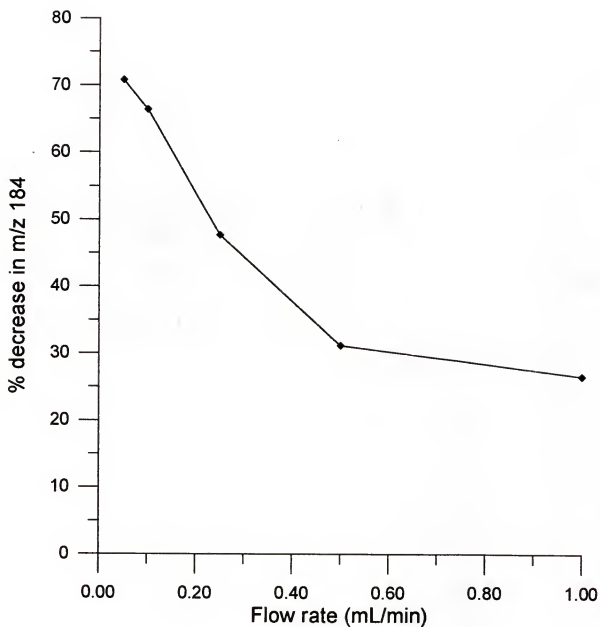


Figure 3.12

Effect of flow rate through the EC cell on electrochemical efficiency for the conversion of benzidine; plotted is decrease in m/z 184 intensity vs flow rate.

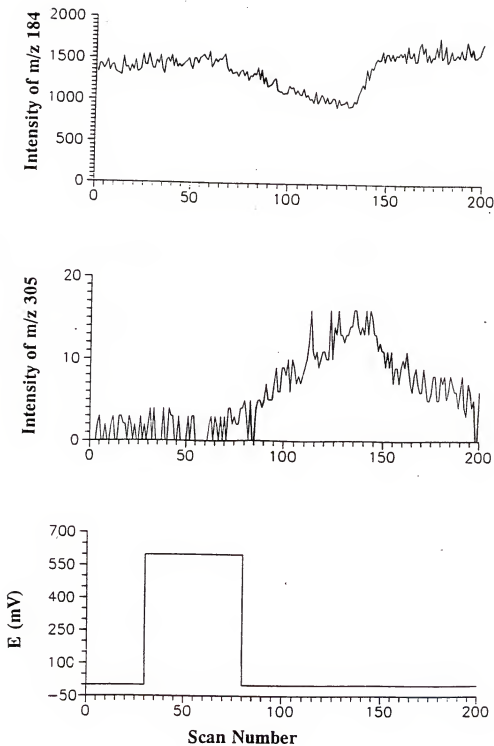


Figure 3.13 EC/PBI/ITMS of benzidine, at 1 scan/s.

of the oxidation of benzidine. Figure 3.14 shows mass spectra of benzidine before and during the EC pulse. The increase in the product ion signal is much less than the observed decrease in benzidine ion signal. The relatively low amount of product observed is thought to be due to loss of other product species such as polymers of benzidine (and perhaps most of this product as well), through adsorption to the electrode material or losses in the PBI transport process to the mass spectrometer. The relatively low level of the product formed is also seen in the mass spectrum taken during the EC pulse where the  $m/z$  305 intensity is less than 2% of the base peak. While the electrochemical conversion here is quite low, recall that no oxidation products were observed in the EC/TSP/MS experiments for benzidine discussed previously in Chapter 2.

Using methanol chemical ionization to enhance the "molecular" region of the spectrum, EC/PBI/MS was again performed on benzidine. Figure 3.15 shows mass spectra of benzidine using methanol chemical ionization before and during application of a potential to the EC electrode. The product at  $m/z$  305 was again observed as the only species whose mass chromatogram increases concurrent to an observed decrease in benzidine ion signal, but the relative intensity of  $m/z$  305 had increased to approximately 5% of the base peak. The increase in relative intensity of the  $m/z$  305 product while using chemical ionization suggests that this is indeed a protonated species that is formed even when electron ionization conditions are used due to the large amount of solvent present in the ion trap and the relatively long times available for reaction between solvent ions and product neutrals.

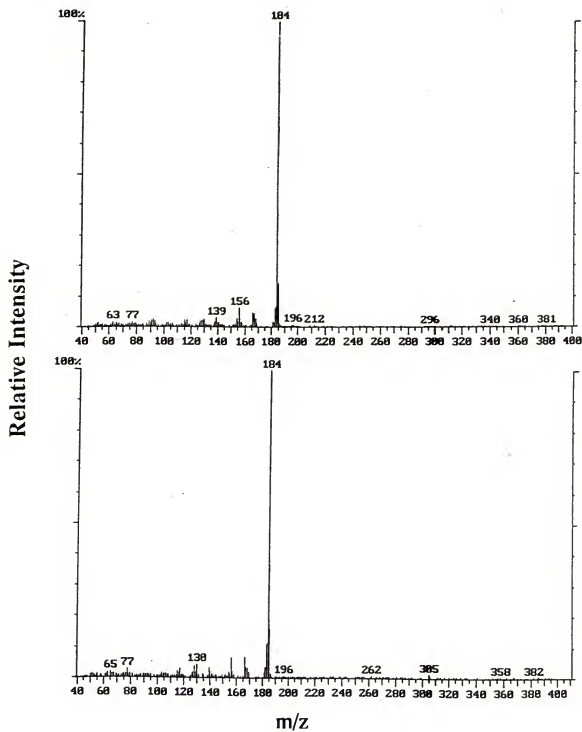
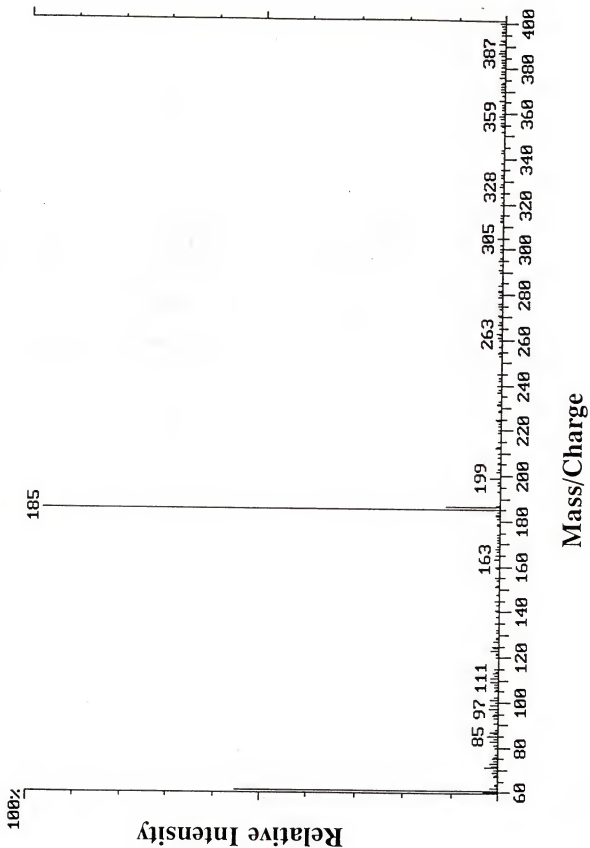


Figure 3.14 Mass spectra taken during EC/PBI/ITMS of benzidine at scan number a) 35 and b) 135.

**Figure 3.15** Methanol chemical ionization mass spectrum of benzidine taken with electrochemical potential of 600 mV vs Pd.

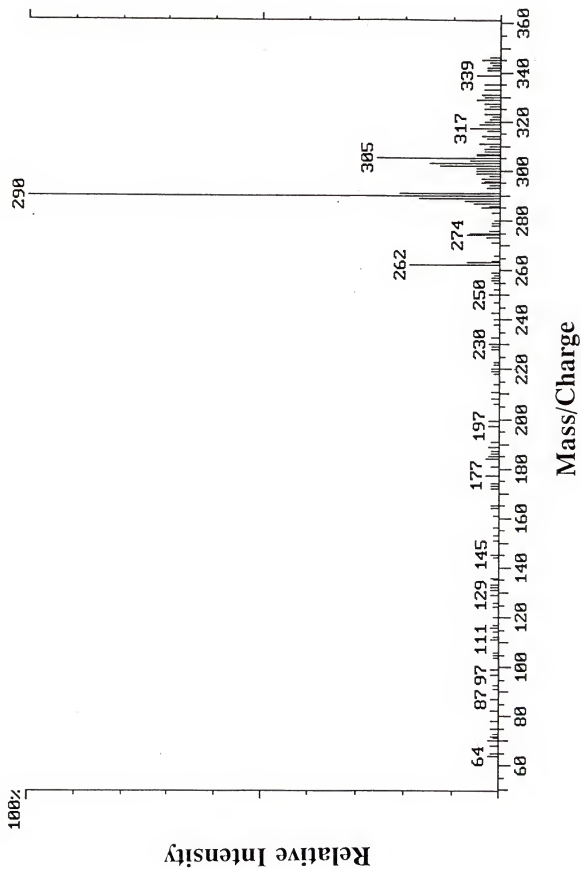


Based on the above observations, it was proposed that the  $m/z$  305 ion was protonated  $N,N,N',N'$ -tetramethoxy benzidine. Tandem mass spectrometry (MS/MS) of the  $m/z$  305 species was then performed to support the identification of this ion with the EC electrode poised at +600 mV vs Pd. A daughter ion spectrum for  $m/z$  305 from EC/PBI/MS/MS of benzidine is shown in Figure 3.16. The major daughter ions of  $m/z$  305 are at  $m/z$  290 and  $m/z$  262. The  $m/z$  290 ion corresponds to the neutral loss of 15 u, presumably a methyl group, and the  $m/z$  262 ion, corresponding to a loss of 43 u from the original ion, could be from loss of CHON. The losses observed during MS/MS are reasonable for the proposed oxidation product. MS/MS/MS was attempted on each of the daughter ions,  $m/z$  290 and  $m/z$  262, but no additional information was obtained due to the low signal intensities of each of these daughter ions.

Substituted benzidines, 3,3'-dichlorobenzidine and 3,3'-dimethyl benzidine (o-tolidine), were also studied by EC/PBI/MS. These compounds exhibit the same electrochemical behavior as benzidine when examined by cyclic voltammetry, so the same potential used for benzidine EC/PBI/MS experiments was used for these. In the mass chromatogram a decrease in the molecular ion ( $m/z$  212) of more than 50% is observed during the application of the electrochemical pulse. However, no oxidation products are apparent in the mass spectra. Experiments using dichlorobenzidine produced the same results: a large decrease in molecular ion was observed although no products were seen.

**Figure 3.16** Daughter spectrum of oxidation product of benzidine at  $m/z$  305.



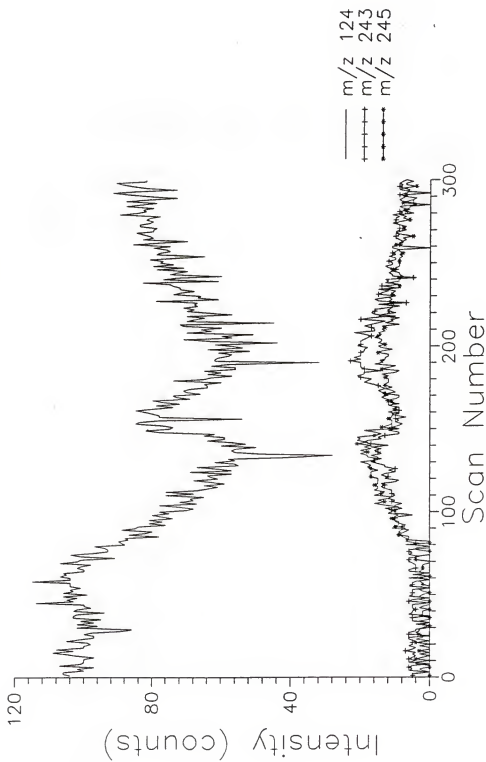


EC/MS was also performed on anisidine (p-methoxyaniline). The molecular ion signal for anisidine was low using electron ionization, so methanol chemical ionization was used for those EC/MS experiments. Figure 3.17 shows spectra for anisidine at EC cell potentials of 0.0 V and 0.6 V vs Pd. The appearance of ions at  $m/z$  243 and  $m/z$  245 in the second spectrum suggest the formation of azo- and hydrazo-derivatives of anisidine. The amount of product ions, although much greater than that observed in the case of benzidine, still does not equal the loss of molecular ion.

EC/PBI/MS of aniline was also attempted. Aniline is significantly more volatile than the benzidines or anisidine, and the increased volatility poses some additional challenges for PBI/MS. Highly volatile compounds can be completely vaporized in the desolvation chamber and pumped away in the momentum separator, so lower desolvation chamber temperatures must be used. The use of an aqueous solvent system was not possible; even a mixed solvent required a desolvation chamber temperature too high to allow transport of aniline. Using 0.01 M  $\text{NH}_4\text{CH}_3\text{COO}$  in methanol, EC/PBI/MS was performed on aniline. The mass chromatogram of the molecular ion of aniline is shown in Figure 3.18. The intensity of  $m/z$  93 increases with the application of the positive potential to the cell, but the mass spectrum remains unchanged. The increase in  $m/z$  93 intensity indicates some change is occurring, but any electrochemical transformations which occur do not result in any changes in the mass spectrum; one possible explanation is that the

**Figure 3.17**

EC/PBI/ITMS of anisidine, at 1 scan/s; plotted are mass chromatograms for  $m/z$  124 (protonated anisidine), and  $m/z$ 's 243 and 245 (protonated azo- and hydrazo- products).



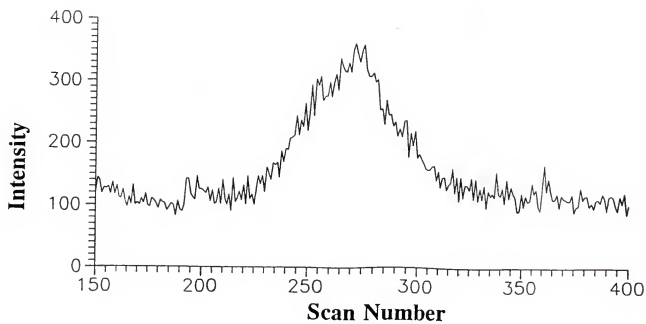


Figure 3.18

EC/PBI/ITMS of aniline; plotted is the mass chromatogram for the molecular ion of aniline.

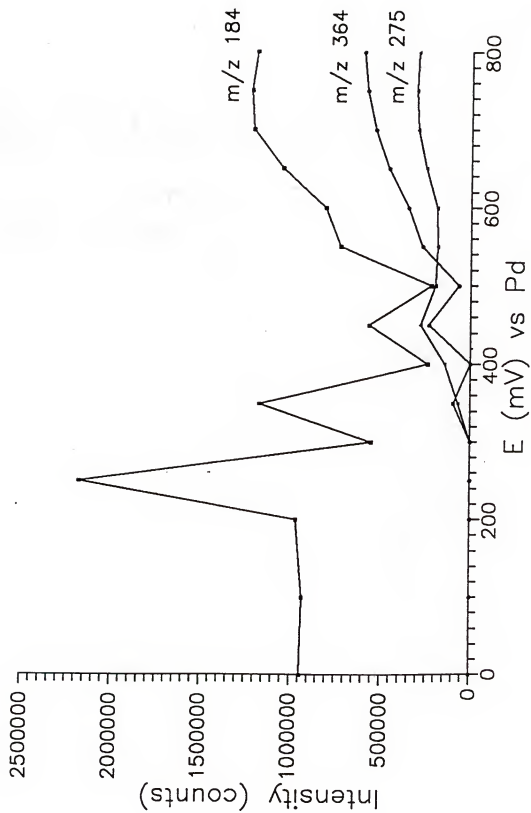
electrochemically generated products thermally decompose upon striking the heated endcap to regenerate aniline.

#### Electrochemistry/Particle Beam/ITS40

The use of an external ion source for PB/MS greatly reduces any effects of the solvent. The amount of solvent neutrals reaching the ion trap is significantly reduced because the particle beam is not directed into the trap; the lower solvent background leads to fewer reactions between solvent species and analyte species. EC/PBI/MS was performed on benzidine using the modified ITS40 system discussed previously in this chapter. The MSHV obtained using this instrument is shown in Figure 3.19. This set of experiments is similar to those performed on benzidine using TSP/MS except that the solvent system was 50/50 methanol/water rather than 100% aqueous; a new EC cell was used in these experiments because the backpressure associated with the old cell had exceeded the operating pressures of the HP 1090 liquid delivery system. The MSHV shows intensity data for the molecular ion of benzidine ( $m/z$  184) and two apparent product species at  $m/z$  275 and  $m/z$  364; mass spectra at 0 mV and 700 mV vs Pd are shown in Figure 3.20. Possible structures for the electrochemically generated products are shown in Figure 3.21. The formation of azo-derivatives was observed in EC/PBI/ITMS experiments of anisidine (Figure 3.17) and is consistent with the chemistry of this class of compounds [36].

These results for the MSHV of benzidine are significantly different from those seen using TSP/TQMS or PB/ITMS systems. The MSHV obtained using

**Figure 3.19** Mass spectrometric hydrodynamic voltammogram of benzidine obtained on EC/PBI/TTS40 system.





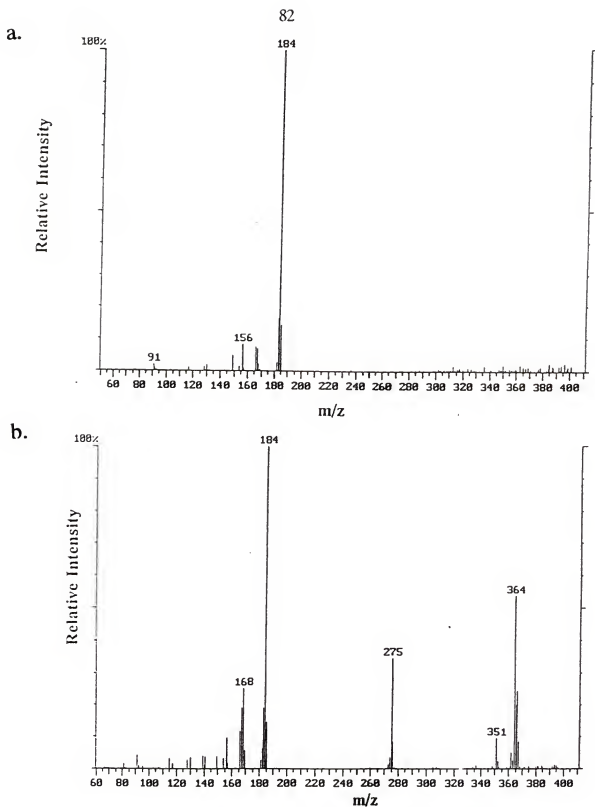
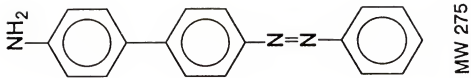


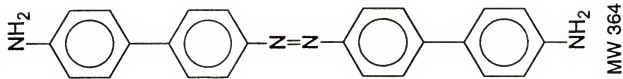
Figure 3.20 Mass spectra of benzidine at a) 0 mV and b) 700 mV vs Pd.

Figure 3.21

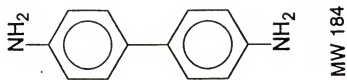
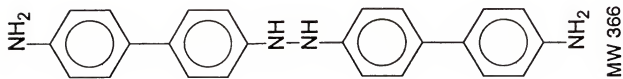
Possible structures for the oxidation products observed in the EC/PBI/ITS40 experiments with benzidine.



+



+



EC/TSP/TQMS showed decreases in the intensities of all ions associated with benzidine (protonated and other adducts) but no increases in any ions which could be products; the EC/PBI/ITMS experiments using infusion of the sample had a product, N,N,N',N'-tetramethoxy benzidine, which had undergone significant reaction with the methanol in the solvent; reactions between oxidized species and nucleophiles such as ammonia, have been observed in previous EC/MS work [17]. The differences in the observed EC/MS behavior among the systems may relate to certain experimental factors: flow rate, solvent system, and condition of the electrode. The flow rate, which directly affects the residence time of the analytes in the EC cell, used in EC/PBI/ITS40 experiments was greater than that used in EC/PBI/ITMS work but less than that used in EC/TSP/MS (flow rates of 0.25, 0.1, and 1.0 mL/min, respectively). Higher flow rates result in less time for reaction to occur both at the electrode surface and in the solution in the tubing between the EC cell and the interface. The solvent systems used differed between experiments using the PBI vs the TSP. The lack of methanol in the TSP system leads one to expect differences in products because methanolysis could not occur without methanol in the solvent system. The solvent systems were, however, the same in EC/PBI/ITMS and EC/PBI/ITS40 experiments. The EC/PBI/ITS40 experiments were performed with a new electrochemical cell. The cell in use had been fouled substantially as seen in the very high backpressures after many experiments (initially pressures of 100-150 psi, later over 4000 psi), and this fouling may have altered its electrochemical or physiochemical properties by altering the surface of the electrode.

The MSHV was repeated on benzidine with the new electrochemical cell using the EC/PBI/ITS40 system but now in a 100% aqueous solvent system; Figure 3.22 shows the results for these experiments. The figure shows plots of the peak area of the molecular ion of benzidine ( $m/z$  184) at various potentials over the range of interest; each point is the average of three injections. The intensities of benzidine molecular ion for the mixed solvent system is higher than for the aqueous system demonstrating the improvement in PBI operation when organic solvents are used. As with EC/TSP/MS experiments, no electrochemical products were observed in the experiments using a 100% aqueous solvent system.

### Conclusions

The experiments involving EC/PBI/MS yielded a variety of results. Benzidine and substituted benzidines reacted strongly in EC/PBI/ITMS experiments, as evidenced by the large decreases in molecular ion signals when the electrode was poised at a potential for oxidation, but very little, if any, products were detected. The production of N,N,N',N'-tetramethoxybenzidine was observed consistently during the oxidation of benzidine, and EC/PBI/MS/MS was used to support the preliminary identification of this species. This product was not observed in EC/PBI/ITS40 experiments which used a new (unfouled) electrochemical cell; rather, azo- and hyrazo- products were observed. Significant differences in the observed products for EC/MS of benzidine were also noted with the use of different solvent systems. The use of an aqueous solvent system for benzidine (both using EC/PBI/MS and

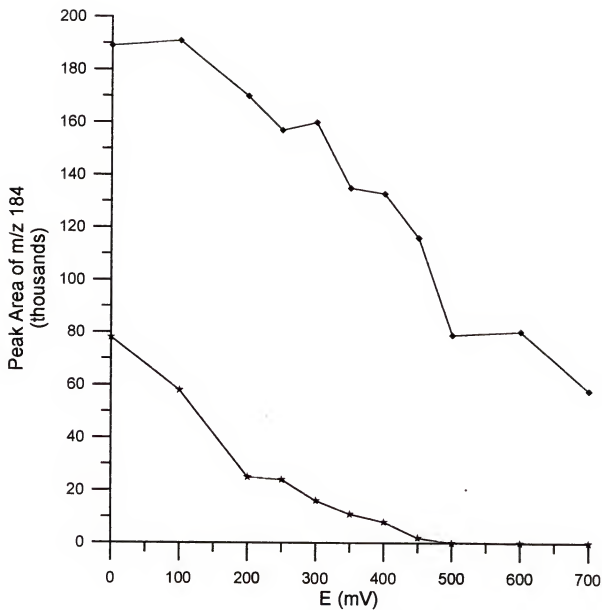


Figure 3.22 Mass spectrometric hydrodynamic voltammograms of benzidine in aqueous and mixed (methanol/water) solvent systems using EC/PBI/ITS40 system; the mass chromatogram of  $m/z$  184 (benzidine molecular ion) is plotted for each solvent system.

EC/TSP/MS) yielded no observable electrochemical products. The decrease in molecular ion signal for benzidine followed the same pattern (same potentials of oxidation) in either aqueous or mixed (methanol/water) solvent systems.

The EC/PBI/ITMS of anisidine (conducted with the "old" cell) also produced azo- and hydrazo-derivatives. The amount of product observed in each of this case was much greater than that observed in the formation of N,N,N',N'-tetramethoxy-benzidine. EC/PBI/MS of aniline yielded a surprising result; the signal for aniline increased with the application of the electrochemical potential. It is believed that the electrochemical product(s) of the oxidation of aniline may be more amenable to the PBI transport processes but reform aniline upon striking the heated target. This result is not completely unexpected, since electrochemistry has been used with thermospray and fast atom bombardment to improve various analytes' responses in these interfaces.

## CHAPTER 4

### IMPROVED ION DETECTION EFFICIENCIES FOR IONS STORED IN A QUADRUPOLE ION TRAP

#### Introduction

The quadrupole ion trap was first disclosed by Paul in the 1950's [22]. For many years the quadrupole ion storage device, or QUISTOR, was used primarily as a reaction vessel for spectroscopic studies of ions [37]. The ion trap was also used as an ion source for other mass analyzers, with ions created in the QUISTOR ejected into the mass analyzer by a DC pulse applied to one or both endcap electrodes [38,39]. Recent experiments using an ion trap as a source for a time-of-flight mass spectrometer have utilized removal of the RF trapping field during application of an extraction pulse applied to an endcap [40]. In each of these cases a DC pulse applied to an endcap has been employed to effect ejection of ions of all mass-to-charge values into the mass analyzer.

The development of mass-selective instability scanning by Stafford et al. of Finnigan MAT [41] made the ion trap a true mass spectrometer with ions created and manipulated (mass isolated, reacted, dissociated, etc) within the trap and then ejected according to their mass-to-charge to a detector. In this mode of operation, ramping the RF trapping field causes ions of increasing mass to be sequentially ejected through an endcap to a detector. The storage, mass isolation, and ejection



of ions are controlled simply by altering the RF and DC voltages applied to the ion trap under computer control. Here we present a remarkably sensitive method for ejecting ions from the trap by removing the RF trapping field [42].

### Experimental

All rapid removal of RF experiments were performed on a Finningan ITMS quadrupole ion trap mass spectrometer using Ion Catcher Mass Spectrometer (ICMS) software developed in this laboratory [32]. The ICMS software provides a number of unique capabilities on the ITMS, including the detection of ions at times other than an RF ramp and the collection of profile data. In some experiments, a LeCroy model 9400 digital storage oscilloscope was used to collect ion signal directly from the pre-amp on the ITMS. Simulations of the ion trajectories were performed using ITSIM [43] running on a Compaq 486/33 MHz personal computer.

Due to the non-mass selective nature of this ion ejection method, a single mass-to-charge was isolated in the ion trap prior to ejection; mass isolation was effected by using a two-step RF/DC isolation procedure [24]. In this isolation procedure, ions of higher  $m/z$  are removed by addition of a positive DC voltage with the desired  $m/z$  at a  $q=0.4$ ; the RF is then ramped to place the desired  $m/z$  at  $q=0.89$ , and a negative DC pulse is applied to remove lower  $m/z$  ions. A stability diagram illustrating the isolation method is shown in Figure 4.1. The scan functions used in these studies utilized ionization of the sample at an RF voltage corresponding to a Mathieu parameter for the molecular ion of  $q=0.2$ , isolation of

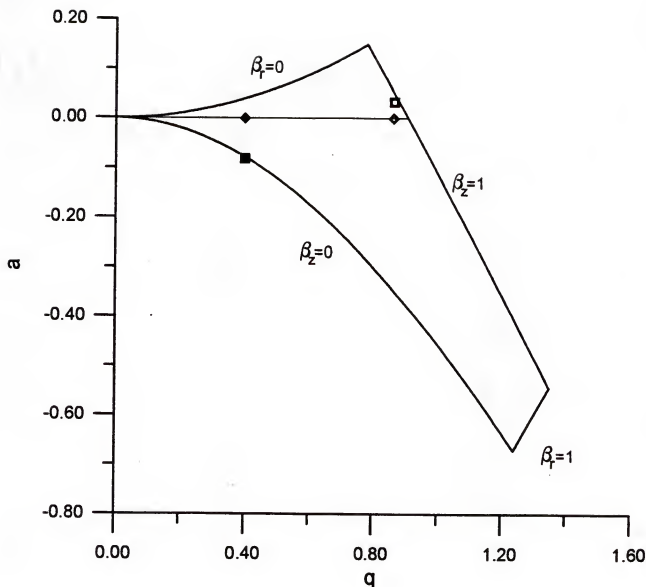


Figure 4.1

Mathieu stability diagram illustrating the two-step isolation procedure. The solid diamond indicates the  $a, q$  position of ion storage prior to isolation. The solid square shows the  $a, q$  position for removal of higher  $m/z$  ions. After removal of higher  $m/z$  ions the RF would be ramped to the position indicated by the open diamond, and lower  $m/z$  ions would be removed with a DC pulse ( $a, q$  position indicated by the open square).

the  $m/z$  of interest, then cooling for 20 ms at a constant RF voltage (an optimized  $q$  value) prior to ejection/detection. For comparison studies, the scan functions for detection by rapid removal of the RF and by mass-selective instability were identical until the detection table. Examples of the scan functions used in this work appear in Figure 4.2.

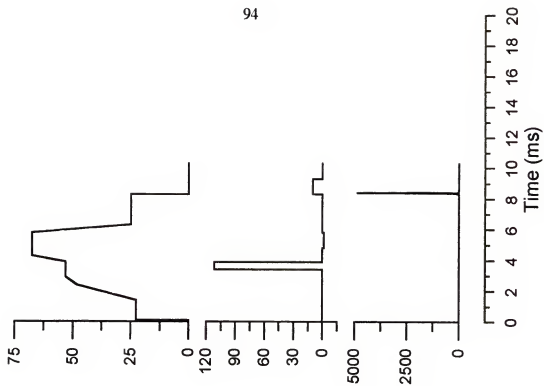
### Characterization of Detection by Rapid Removal of RF

A digital storage oscilloscope was connected to the preamp test point on the ITMS to examine the ion peaks produced by using rapid removal of RF. The RF detector was also monitored using the DSO. Argon was used initially so no mass isolation was necessary; argon produces no ions above  $m/z$  40 ( $\text{Ar}^+$ ), and lower  $m/z$  ions (e.g., from air and water) are removed by ramping the RF to a low-mass cutoff of 34 u prior to detection. The fundamental characteristics of the ejection process, such as peak width and time required for ejection, were examined. Figure 4.3a shows DSO traces of the RF DAC out (bottom) and preamp signal (middle and top) for acquisition using rapid removal of RF with +5 V DC during acquisition. Two cycles of the experiment are shown in the figure; the top trace is the second cycle with the time scale expanded by a factor of 50. These data were collected without the addition of helium buffer gas. The figure indicates that the argon ion peak width is approximately 100  $\mu\text{s}$  at the base. The addition of helium to the ion trap acts to "cool" the stored ions into a smaller packet during the storage period. This is evident in the data of Figure 4.3b; the peak width in this case is decreased to approximately

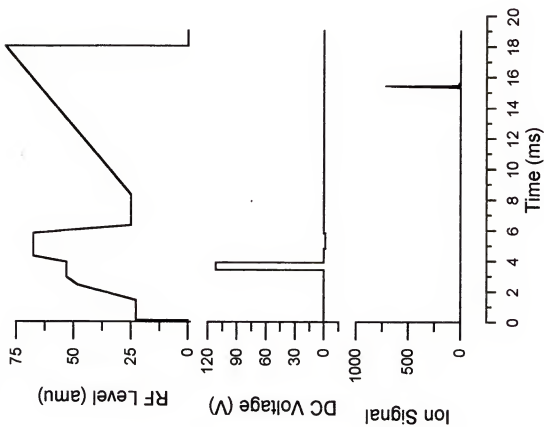
Figure 4.2

Scan functions used for experiments comparing (a) mass-selective instability scanning to (b) detection by rapid removal of the RF. Shown are scan functions for  $m/z$  69: ionization of  $q=0.2$  (0-1 ms), two-step isolation of  $m/z$  69 (1-6 ms), cooling at  $q=0.25$  (6-8 ms), then ejection and detection ( $>8$  ms). Plotted (top to bottom) are the RF trapping voltage (shown as the low  $m/z$  cutoff), the DC voltage applied to the ring, and the detected ion signal.

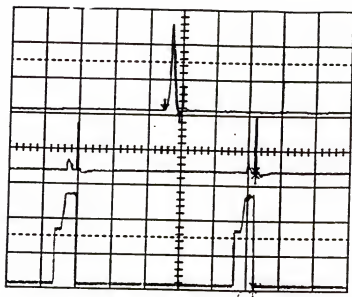
b.



a.



a.



b.

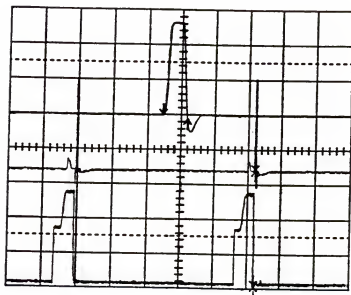


Figure 4.3

DSO traces of RF DAC out and preamp signal for argon ions ( $m/z$  40) a) with no helium buffer gas and b) with helium buffer gas.

75  $\mu\text{s}$  while the ion signal intensity is increased substantially (the exact amount of the increase is indeterminate because the peak is off-scale using helium buffer gas).

The DSO was also used to examine rapid removal of RF with multiple  $m/z$  ions from PFTBA. Figure 4.4 shows the DSO traces for the RF detector and the ion signal measured at the preamp. The ion packet begins to come out approximately 40  $\mu\text{s}$  after the RF begins to decay, and the ion peak is completed in approximately 150  $\mu\text{s}$  after the RF begins to decay. It is interesting to note that the RF has not reached a zero level when the ions are being ejected; this fact supports the theory that the ejection process is due to the crossing of a stability boundary, not simply a field-free drift. Some mass resolution is seen as three overlapping peaks appear for the major PFTBA ions (higher mass at shorter time), and the baseline width is significantly wider (approximately 120  $\mu\text{s}$ ) than that observed for ion of a single  $m/z$ . The mass resolution in this case is very poor, because the rate of change of the RF is very fast relative to normal scanning procedures which yield unit mass resolution; this points out the need to perform mass isolation prior to ejection of the ions.

Studies were also performed to examine the timing of the RF command signals and the time required for ions to "drift" out of the trap. A scan function was used in which the RF level was pulsed to zero during the ion storage period; details of this scan function were given previously in this chapter. DSO traces for the RF DAC out and preamp signal are shown in Figure 4.5. In the top figure, the time for the pulse of the RF to zero is set at 0  $\mu\text{s}$ ; however, the trace shows that the pulse is actually approximately 110  $\mu\text{s}$  in duration. During this time in which the RF is at

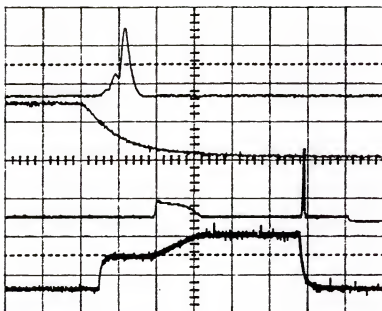


Figure 4.4

DSO traces of RF detector and preamp signal for PFTBA ions without mass isolation. Horizontal scales for traces from top to bottom: 0.1 ms/div, 0.1 ms/div, 1 ms/div, 1 ms/div. Vertical scales for traces from top to bottom: 5 V/div, 0.2 V/div, 5 V/div, 0.2 V/div.



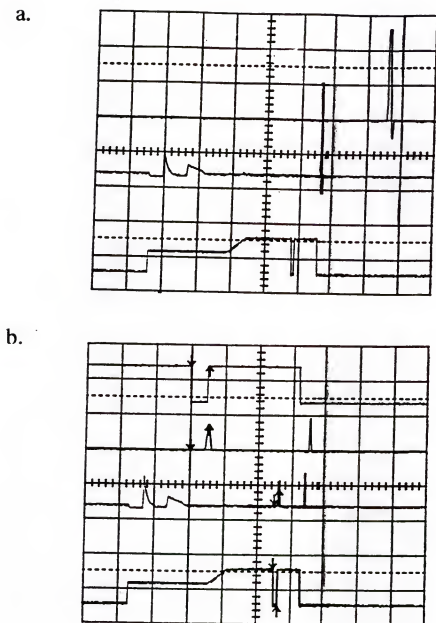


Figure 4.5

DSO traces of RF DAC out and preamp signal for scan functions with an RF pulse to zero during the ion storage period; a) RF pulse set to  $0\ \mu\text{s}$ , b) RF pulse set to  $100\ \mu\text{s}$ . Horizontal scale:  $2\ \text{ms/div}$  (bottom and middle),  $0.5\ \text{ms/div}$  (top); vertical scale:  $0.5\ \text{V/div}$ ,  $5\ \text{V/div}$ ,  $5\ \text{V/div}$  (bottom to top).

zero, no ion signal is observed on the preamp trace indicating that with no DC voltage applied to the ring electrode ions do not reach instability in the 100  $\mu$ s time period observed, and a significant peak is observed during the acquisition time (RF to zero at the end). In the bottom figure, the time for the RF pulse is set to 100  $\mu$ s, and the observed time is 210  $\mu$ s. This data show that a significant portion of the ion signal which would normally appear in the acquisition time is observed during the time the RF is set to zero. The traces show that there is approximately 110  $\mu$ s added to the time of the table in which the RF is set to zero; this time does depend on what other functions are being performed during the same table, but the time is somewhat longer than requested.

Studies were performed to optimize the ion signals obtained by rapid removal of the RF; the signal initially obtained was very low and almost indistinguishable from the background. More intense ion signals were observed if a positive DC voltage was applied to the ring electrode during the table in which the RF voltage was set to zero. Figure 4.6 shows a comparison of ion signals for the  $\text{CF}_3^+$  fragment ion ( $m/z$  69) of perfluorotributyl amine (PFTBA) with and without a positive DC voltage applied to the ring. As the data show, application of even a modest positive DC voltage results in a dramatic increase in ion signal (note the 100x difference in intensity scales).

The effect of the DC voltage applied to the ring on the timing and intensity was also examined with argon ions. Figure 4.7 shows DSO traces of the preamp ion signal for argon with and without the application of a positive DC voltage during the

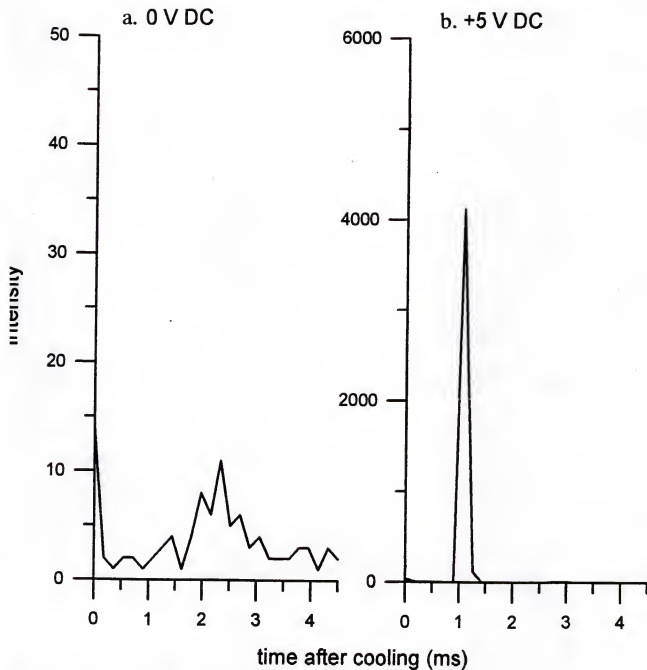
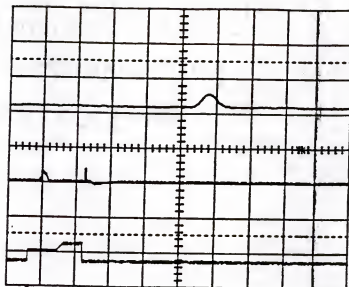


Figure 4.6

Ion signal obtained by rapid removal of RF for  $m/z$  69 ion from PFTBA a) without DC and b) with DC voltage applied to the ring electrode during the ejection time.

a.



b.

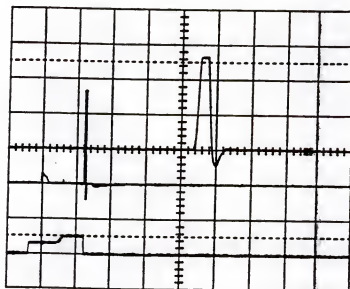


Figure 4.7

DSO traces of RF DAC out and preamp signal for argon ions without and with DC voltage applied to the ring electrode during the ejection time. Horizontal scales for traces top to bottom: 5 V/div, 5 V/div, 1 V/div. Vertical scales for traces top to bottom: 0.1 Ms/div, 5 ms/div, 5 ms/div.

acquisition. The ion peak with DC voltage is dramatically larger than the peak without DC, although the full extent of the increase cannot be determined since the preamp was at maximum output voltage for this large number of ions. It is also interesting to note that the ion peak in the case with DC comes out approximately  $20\ \mu\text{s}$  earlier.

To help explain this observation, the effect of DC voltage during RF removal on the  $m/z\ 69$  ions stored in the trap was simulated using ITSIM [43]. Figure 4.8 shows ITSIM results for  $m/z\ 69$  ions during removal of the RF trapping field (a) without and (b) with DC applied to the ring. In the figure, the top graph shows the RF and DC voltages applied to the ring electrode; the RF voltage is shown approximating an exponential decay, as was observed for the ITMS. Ion trajectories in the  $x$  and  $z$  directions are shown;  $x$  trajectories are related to the radial ( $r$ ) motion of ions in the ion trap since  $r^2 = x^2 + y^2$ , whereas  $z$  trajectories are in the direction of the endcaps. The simulation assumes the theoretical (unstretched [44]) geometry of the ion trap, with a ring electrode radius ( $r_0$ ) of 1.0 cm and a center-to-endcap distance ( $z_0$ ) of 0.7 cm. The bottom trace indicates the kinetic energies of the ions. The simulations in Figure 4.8a and b indicate an increase in ion detection efficiency for a detector positioned behind one endcap electrode is expected when a positive DC voltage is applied to the ring electrode, because the ions become unstable axially (in the  $z$  direction) with the application of positive DC voltage, rather than radially (in the  $x$  direction) as is the case when no DC is used.

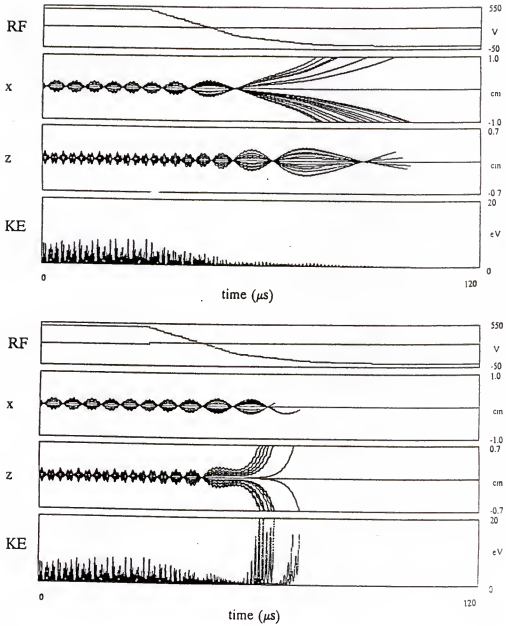


Figure 4.8

ITSIM simulation of rapid removal of RF (a) without and (b) with DC voltage applied to the ring electrode during the ejection time.

The increased detection efficiency can be explained in relation to the Mathieu stability diagram, shown in Figure 4.9 [23]. When a positive DC voltage is added to the ring, the ions are at a negative Mathieu  $a$  parameter; when the RF is turned off, the decay of the RF (Mathieu  $q \rightarrow 0$ ) causes the ions to cross the lower left Mathieu stability boundary at  $\beta_z = 0$ . The ions thus become unstable in the  $z$ , or axial, direction and are ejected toward the endcap electrodes (behind one of which is situated the detector). In the case where no DC is added (Mathieu parameter  $a=0$ ), the ions do not cross any instability boundary; ITSIM indicates that the ions become unstable primarily in the radial direction and subsequently are ejected toward the ring electrode (Figure 4.8a). The magnitude of the applied DC voltage influences the width of the detected ion packet. ITSIM indicates that the application of +10 V DC causes all  $m/z$  69 ions to become unstable in a significantly narrower time range than does +1 V DC; experiments confirm this prediction. The narrower peak for the detected ions results in a greater peak height and better sensitivity.

In the studies discussed above, the RF level prior to beginning the ejection/detection process was chosen as one which has previously been shown to be an efficient region of ion storage. This level may not, however, be optimum for the operation of the ion trap using rapid removal of the RF. Experiments were thus undertaken to determine if the RF level at which the ions are stored immediately prior to turning the RF off has any effect on the signal observed. The experiments were conducted by using the previously determined optimum DC voltage for each

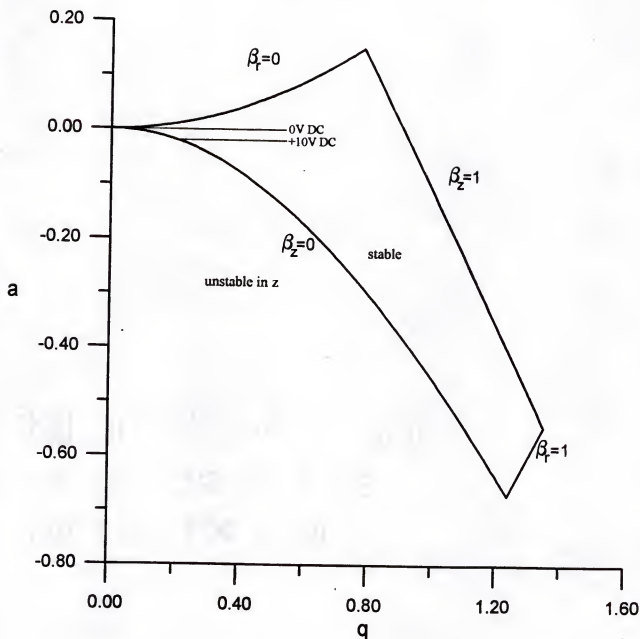


Figure 4.9

Mathieu stability diagram in  $a$ - $q$  space. The parameter  $a$  is proportional to the magnitude of the DC voltage applied to the ring electrode; the parameter  $q$  is proportional to the magnitude of the RF applied to the ring electrode.



$m/z$  studied. For each  $m/z$ , the RF level, represented by the low mass cut-off (LMCO), was incremented by 0.5 amu from 5 amu to the  $m/z$  of the ion of interest.

Figure 4.10 shows plots of ion signal intensity versus the Mathieu parameter  $q$  of the ions immediately prior to removal of the RF. The plots for  $m/z$ 's 69, 131, 264, and 414 show a general trend of increasing intensity to a  $q$  of about 0.6. The plot for  $m/z$  502 is relatively constant over the entire range. All of the traces demonstrate oscillations that become broader as the  $q$  of storage increases; the cause of these oscillations is not yet understood. One interesting point is the sharp minima at  $q=0.65$ . These minima correspond to a  $q$  value previously reported as an octapolar non-linear resonance at  $\beta_z = \frac{1}{2}$  [45]. Other non-linear resonances, around  $q=0.82$ , are seen in the plots for  $m/z$ 's 502, 414, and 264, though these are not as pronounced as the resonance at  $q=0.65$ . These non-linear resonances may cause some of the stored ions to be ejected during the storage period due to the absorption of energy. The loss of ions during the storage period results in subsequent detection of a significantly lower ion signal at these particular RF voltages.

In initial experiments using storage at  $q=0.2$ , the use of DC voltages that result in a Mathieu  $a$  parameter more negative than -0.03 caused ion instability to occur when the DC pulse was applied; ejection of the ions occurs during the application of the DC pulse before the instrument begins its acquisition of data (the collection of data does not begin until the RF is turned off). Figure 4.11 shows oscilloscope traces of the detector output and RF detector for rapid removal of RF for  $m/z$  131 stored at a LMCO of 24 u and stored at a LMCO of 15 u. The lower

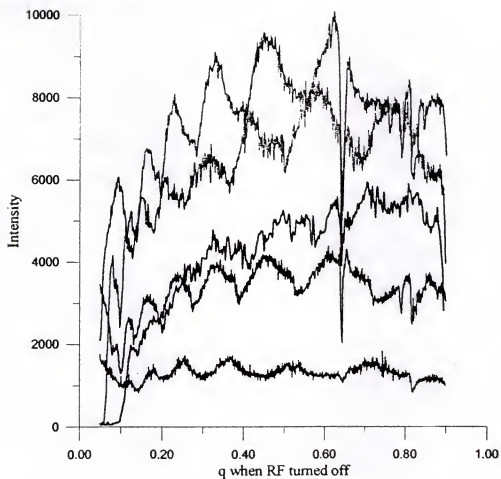
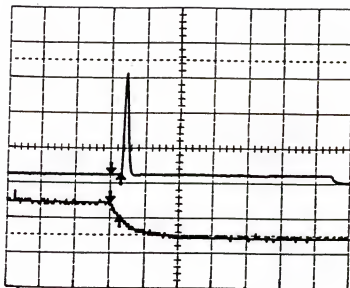


Figure 4.10

Plots of ion signal intensity for  $m/z$ 's 69, 131, 264, 414, and 502 vs. Mathieu parameter  $q$  of the ions immediately prior to the removal of the RF.

a.



b.

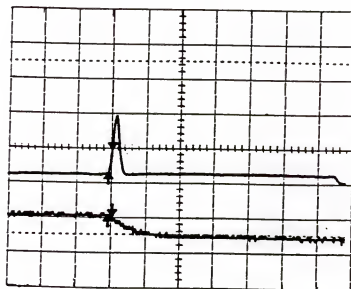


Figure 4.11

DSO traces of the RF detector and preamp signal for  $m/z$  131 stored at a low-mass cutoff of a) 24 amu and b) 15 amu. Horizontal scale 0.2 ms/div. Vertical scale: 2 V/div (top trace), 0.5 V/div (bottom trace).

trace in each plot shows the RF detector output and the upper trace shows the preamp signal. In the case where the ions are stored at a LMCO of 24 u, the ion peak starts 56  $\mu\text{s}$  after the RF begins to decay, thus all of the ion signal will be acquired by the computer. When the ions are stored at 15 u before ejection, however, the ion peak starts 24  $\mu\text{s}$  before the RF decay; in this case approximately 1/3 of the ion signal will be lost by the computer because acquisition will not have yet begun before some of the ions are ejected. Ions are ejected before the RF turns off because the DC voltage is applied before the computer signals the instruments to change the RF, and at low RF storage levels the applied DC voltage causes the stored ions to become unstable.

The storage of ions at higher  $q$  values allows for the use of higher DC voltages during ejection by rapid removal of RF. The effect of DC voltage was examined for  $m/z$  264. The experiments which varied the  $q$  during storage were repeated using various DC voltages; the results are shown in Figure 4.12. The optimum ion intensity for  $m/z$  264 was obtained using a DC voltage of +40 V during the ion ejection period. The position and size of the minima corresponding to the non-linear resonances is not affected by the increasing DC voltage. It has been reported that the effects of non-linear resonances can be amplified when stored ions are subjected to positive DC voltages [45]; however, these effects are observed when the DC is applied over a relatively long time period (several milliseconds), not in the hundred or so microseconds used here. One other point of interest is the oscillations. The position of the peaks in these oscillations shifts dramatically as the

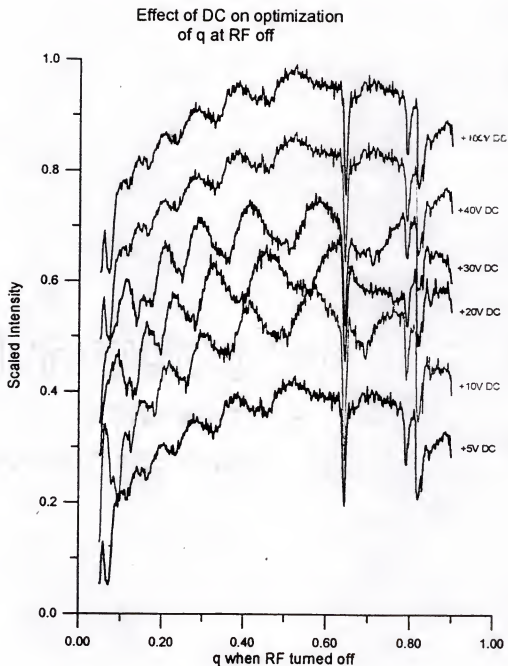


Figure 4.12

Plots of ion signal intensity for  $m/z$  264 vs. Mathieu parameter  $q$  of the ions immediately prior to the removal of the RF using various DC voltages during the ejection time.

DC voltage is changed. The reason for this shift is, as are the oscillations themselves, not yet understood; whatever the cause of the oscillations it would appear that DC voltage applied to the ring has a definite affect on this parameter.

The positions of the sharp minima, presumably corresponding to non-linear resonances, remain constant while the other relative minima and maxima within the oscillatory pattern change their positions in  $q$  space. To provide further evidence linking these sharp minima to non-linear resonances, a study was undertaken to examine the effect of the number of ions on the intensity of these peaks; previous research has shown that the magnitude of non-linear resonance effects is proportional to the number of ions stored within the ion trap [45]. Figure 4.13 shows plots of intensity versus storage  $q$  using increasing ionization times to create larger numbers of ions; all of these experiments were performed using +40V DC applied to the ring during the ejection time. The plot for the lowest ionization time, 0.5 ms, exhibits the distinct oscillations seen in the experiments discussed above, but the sharp minima at  $q=0.65$  is barely observable. As the ionization time, and thus number of ions, is increased the sharp minima become much more apparent, increasing both in depth and width. At an ionization time of 10 ms, the ion signal at the minimum near  $q=0.65$  is reduced by approximately 45% relative to the signal level just before the dip. The minima around  $q=0.78$  and  $0.82$  are also increasing in depth. Also, the oscillation pattern is shifted only slightly as the number of ions is increased.

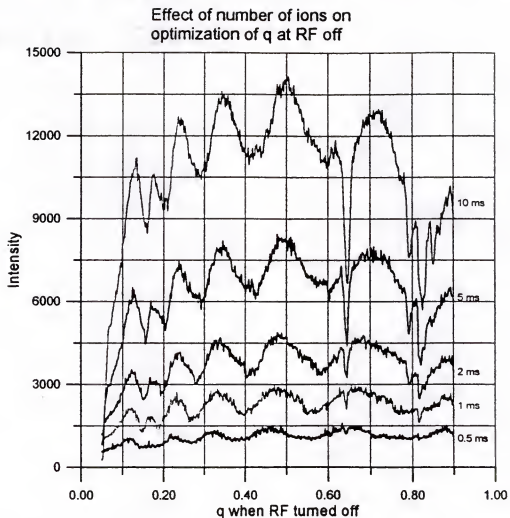


Figure 4.13

Plots of ion signal intensity for  $m/z$  264 vs. Mathieu parameter  $q$  of the ions immediately prior to the removal of the RF using ionization times of 0.5 ms to 10 ms.

### Comparison of Rapid Removal of RF and Mass-Selective Instability Scanning

After initial optimization of the ejection parameters for detection by rapid removal of the RF, the ion detection efficiency obtained by this method was compared with that obtained by mass-selective instability scanning, the standard ejection method used on the ITMS; Figure 4.14 shows a Mathieu stability diagram illustrating each of the ejection methods. In the figure, the diamond represents the point of ion storage prior to the ejection/detection. The line moving to the right from the diamond represents the manner in which mass-selective instability scanning is performed; the line moving down and then left represents effecting ejection by rapid removal of RF. Figure 4.15 shows the ion signals for  $m/z$  40 ions ( $\text{Ar}^+$ ) obtained by each method. In each case, argon was ionized for  $500\ \mu\text{s}$  and  $m/z$  40 was isolated by a two-step RF/DC isolation prior to cooling for 20 ms and ejection/detection. As the figure indicates, a 4-5 times larger signal was obtained by rapid removal of the RF. Table I shows comparisons of ion signals (peak areas) obtained by each method for various ions of PFTBA. It is interesting to note that the signals obtained for higher  $m/z$  ions do not reflect the increases in ion detection efficiency seen for lower  $m/z$  ions. In all cases, the magnitude of the DC voltage was optimized independently for each  $m/z$ , while the parameters relating to ion formation and isolation were held constant. The reason for the mass dependence of the difference between ion detection efficiencies is not apparent; more studies are required to examine these effects.



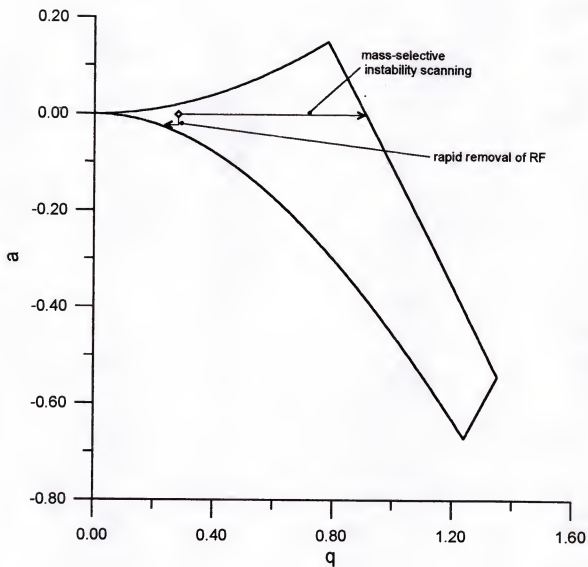


Figure 4.14 Mathieu stability diagram in  $a$ - $q$  space illustrating mass-selective instability scanning and rapid removal of RF.

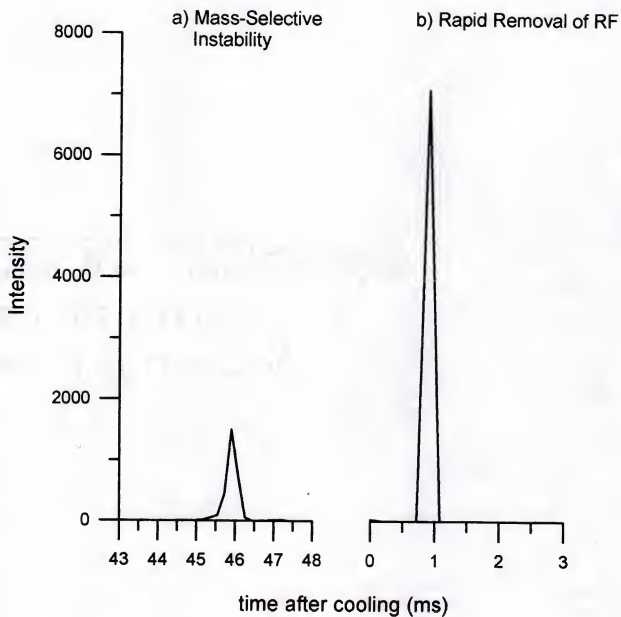


Figure 4.15

Ion signals obtained for argon ions using a) mass-selective instability and b) rapid removal of RF.

TABLE I

Ion Intensities by Mass-selective Instability and Rapid Removal of RF

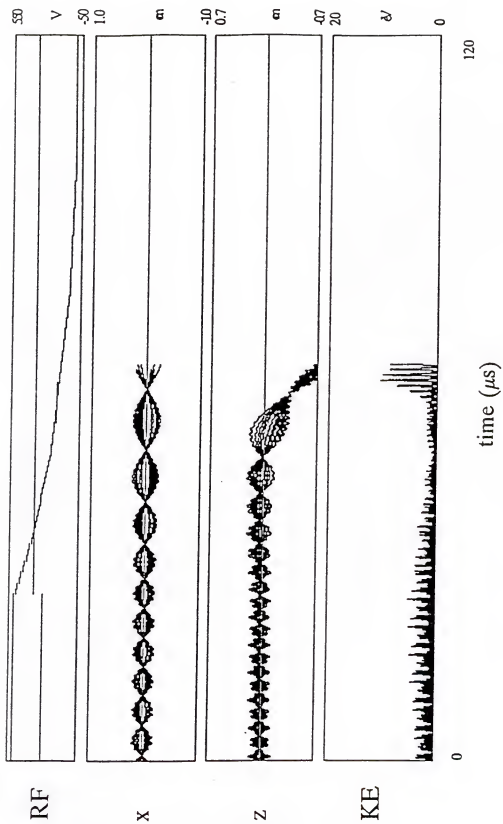
$m/z$	Ion Intensity Obtained by <u>Mass-selective Instability</u>	Ion Intensity Obtained by <u>Rapid Removal of RF</u>
69	795	3755
131	973	2384
264	250	1745
414	545	485
502	82	45

Further Improvements

As seen in simulations, when ions become axially unstable they are ejected toward either endcap. In an effort to gain a factor of two in sensitivity, a means was examined to eject the ions selectively to the endcap behind which the detector is positioned. Although the electronics on the ITMS have no provision for applying a DC differential across the endcaps, the application of AC waveforms of opposite phase to the endcaps is straightforward. By applying a low frequency AC signal (1000 Hz sine wave) through the balun circuit, a differential DC to the endcaps can be approximated since the voltage is essentially constant over the ion ejection period of less than 100  $\mu$ s. A Stanford Research Systems model DS345 waveform generator was used instead of the supplemental AC generator on the ITMS for the application of this signal because the ITMS AC generator does not have a means to set the initial phase of the sine wave. Note that the balun circuit attenuates low frequency waveforms; the 1000 Hz sine wave is attenuated by approximately a factor of 15.

Figure 4.16 shows an ITSIM simulation of rapid removal of the RF with a supplementary AC (1000 Hz sine wave) applied such that the phase of the AC

**Figure 4.16** ITSIM simulation of rapid removal of RF using a supplemental AC voltage (1000 Hz) applied to the endcap electrodes.



waveform is  $90^\circ$  at the time the RF is turned off. The simulation indicates that the ions are ejected toward only one endcap when the phase of the supplemental AC is a multiple of  $90^\circ$ . Studies were performed to determine the dependence of the ion intensities on the initial phase of the AC signal (which affects the amplitude and polarity of the potential across the endcaps at the time of ion ejection). The initial phase of the supplemental AC waveform was adjusted in  $10^\circ$  increments from  $0^\circ$  to  $360^\circ$ . Figure 4.17 shows the results of these experiments; each point is the average of ten scans at each initial phase. The initial phase for the AC voltage is taken to be the phase set on the waveform generator with a phase of  $270^\circ$  corresponding to  $-V_p$  on the detector endcap and  $+V_p$  on the other endcap. The phase set on the waveform generator may not represent the actual phase of the signal on the endcap (due to effects of the balun circuitry and the time delay between the start of the waveform and the time of ion ejection). The difference in the set and actual phases can be seen in the position of the maximum and minimum of the data in Figure 4.17. The expected minimum and maximum would be  $90^\circ$  and  $270^\circ$  respectively; however, the data show a shift of approximately  $25\text{--}30^\circ$  later in phase.

The optimum magnitude of the supplemental AC signal was also examined. The peak-to-peak voltage of the AC signal was taken to be that set on the waveform generator; the set value is not the voltage actually applied to the endcaps due to significant attenuation of the low-frequency signal by the balun box. Figure 4.18 shows the effect of varying the peak-to-peak voltage on the  $\text{CF}_3^+$  ion signal obtained by detection with rapid removal of the RF using supplemental AC. The optimum

Figure 4.17 Plot of ion signal intensity vs. initial phase of the supplemental AC voltage;  $V_{pp} = 400$  mV. Error bars represent  $\pm 1$  standard deviation.

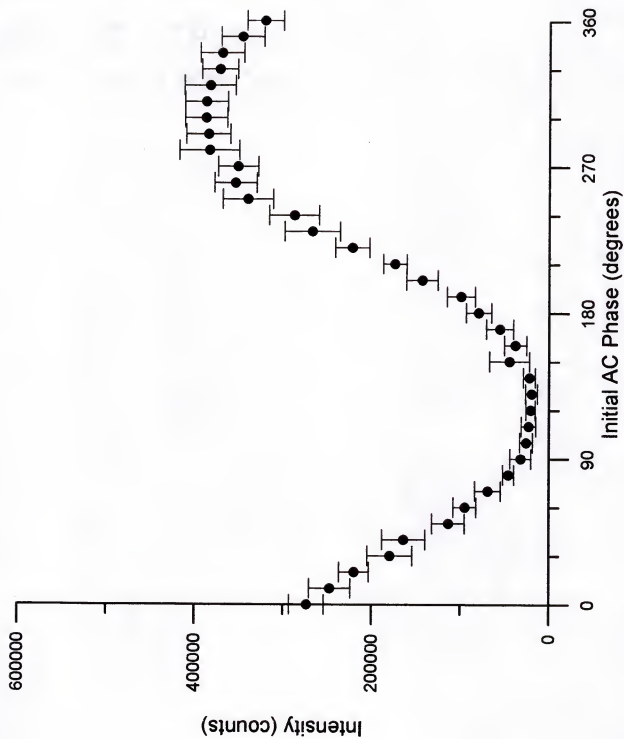
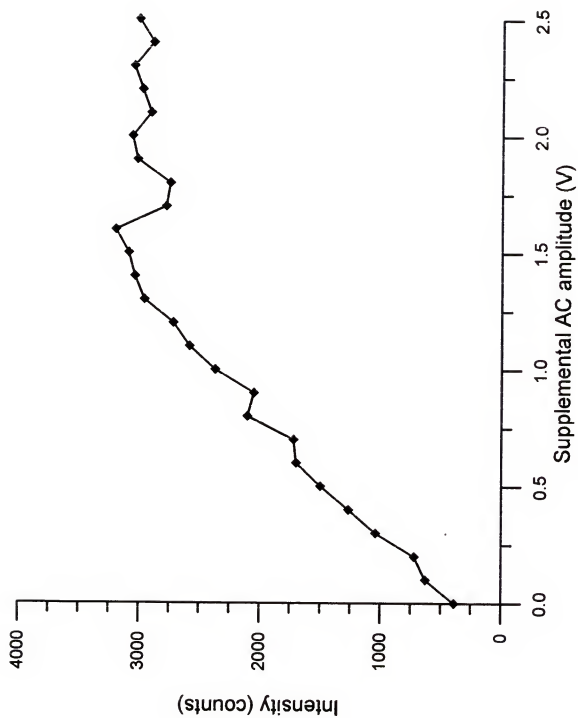




Figure 4.18 Plot of ion signal intensity vs. applied voltage of supplemental AC using an initial phase of  $300^\circ$ .



value for the voltage is approximately  $1.6 V_{pp}$  (as set on the waveform generator); higher voltages produced no significant increases in the ion signal. Whereas an increase in the ion signal by a factor of two (compared to that with no AC) would be expected in these experiments if the ions normally ejected equally to the two endcaps now all leave via the detector endcap, the use of supplemental AC increased the ion signal for  $m/z$  40 by approximately a factor of eight, as seen in Figure 4.18. This increase is in addition to the increase by a factor of five to eight already observed versus mass-selective instability. Thus by using rapid removal of the RF in conjunction with application of DC to the ring and supplemental AC to the endcaps, an increase of approximately fifty fold can be obtained compared to mass-selective instability scanning. Further studies to examine these improvements in ion signal are in progress.

### Conclusions

The use of rapid removal of the RF to effect ion ejection increases the observed ion signal by as much as fifty fold versus traditional mass-selective instability scanning, if used in conjunction with positive DC voltage on the ring electrode and a supplemental AC voltage of appropriate phase and frequency applied to the endcaps. This leads to the startling conclusion that only a small fraction, in some cases less than 2%, of the ions created and stored in the ion trap are being effectively ejected to the detector by mass-selective instability scanning methods. The increase in ion signal by using rapid removal of RF does not

represent more ions in the trap but more efficient ejection of these to the detector. The increase in detected ion signal could be useful in improving the sensitivity of selected ion monitoring and selected reaction monitoring applications where a relatively small number of specific mass-to-charge ions are important in the analytical determination.

## CHAPTER 5

### CONCLUSIONS AND FUTURE WORK

This dissertation has reported on the use of electrochemistry on-line with mass spectrometry to examine the degradation of a group of environmental contaminants. The use of two different liquid chromatography/mass spectrometry systems was examined, and the operating characteristics of each was compared with the other. Also, a novel mode of ion detection for the quadrupole ion trap has been characterized and compared with the standard mode of ion detection. The significance of this work is three-fold: first, the use of PBI and TSP liquid interfaces allows use of a wider range of liquid flow rates and solvent compositions than available with either interface alone; second, the use of MS/MS and  $MS^n$  provides structural information about the electrochemically generated species; third, the use of a different ion ejection/detection method with the ion trap provides increased sensitivity which could be beneficial in trace analysis applications which employ selected ion/reaction monitoring.

Aromatic amines (aniline, substituted anilines, and benzidine) were chosen to serve as the class of compounds to be examined by electrochemistry/mass spectrometry. None of the compounds chosen were amenable to both PBI/MS and TSP/MS. Thermospray was used for benzidine and dimethyl aniline in aqueous solution; the particle beam interface was used for benzidine, substituted benzidines, aniline, and anisidine. The TSP/MS spectra of the amines yielded protonated

molecular ions and adduct ions formed by reaction of the amines with other ionic species produced by the TSP process. PBI/MS spectra are of two types: (1) electron ionization spectra which include molecular and fragment ions; (2) chemical ionization spectra which yield predominantly protonated molecules.

Electrochemistry/thermospray/triple quadrupole mass spectrometry was demonstrated on benzidine and N,N-dimethyl aniline by producing a mass spectrometric hydrodynamic voltammogram (MSHV) for each compound. The MSHV for benzidine showed significant oxidation of the benzidine, seen in the decrease in signal for protonated benzidine at higher potentials, but no production of other species. It was postulated that the electrochemically generated products from benzidine oxidation were not being transported to the mass spectrometer either due to adsorption on the electrode material or due to ineffective thermospray ionization of these species. Dimethyl aniline had an MSHV which showed decrease in the monitored adduct ion ( $m/z$  181) and increases of other ions ( $m/z$ 's 213, 227, 241), presumably electrochemically generated products, as the EC potential was increased. The major products observed in the MSHV for DMA, specifically dimers of DMA, were similar to those reported in previous work; however some species, producing ions at  $m/z$ 's 213 and 227, were observed which do not correspond to the products reported earlier.

Electrochemistry/particle beam/quadrupole ion trap mass spectrometry was also used to study the amines. Two ion trap instruments were used in the experiments: a standard Finnigan ITMS using internal ionization and a modified

Finnigan ITS40 using an external ion source. EC/PBI/MS was accomplished by different means on the two systems. The ITMS system used a syringe pump with continuous infusion of the sample, while the ITS40 system utilized loop injection of the sample.

EC/PBI/ITMS was performed on benzidine, 3,3'-dimethyl benzidine, 3,3'-dichlorobenzidine, anisidine, and aniline. Benzidine produced a methoxylated product (from reaction with the methanol solvent) under the conditions used in these experiments; however, the amount of observed product was much less than the observed decrease in signal for the parent compound. The substituted benzidines also showed significant losses of parent compound intensity with the application of an oxidative potential, but no products were observed. Anisidine produced azo- and hydrazo-derivatives and in much greater quantity than was observed in the benzidine experiments, although the increase in product signal still did not equal the decrease in signal for the original compound. EC/PBI/ITMS of aniline yielded results different from earlier experiments: the aniline signal increased when the potential was applied to the EC cell. The increase in signal without apparent changes in the mass spectrum indicate that the aniline is probably being converted electrochemically into a species more amenable to the PBI process, and this species reforms aniline during the vaporization process via some thermal reaction.

Benzidine was also examined by EC/PBI/ITS40. Mass spectrometric hydrodynamic voltammograms were created for benzidine in mixed organic/aqueous and aqueous solvent systems. The MSHV obtained using the mixed solvent system

yielded significantly different results than those obtained in aqueous media by EC/TSP/TQMS. Products were observed which correspond to species produced by the formation of azo- and hydrazo-linkages.

The use of electrochemistry on-line with mass spectrometry has been shown to be a satisfactory method for the examination of oxidative pathways modelling metabolism. The use here of a quadrupole ion trap as the mass analyzer demonstrates how this technique can be further extended. The ion trap allows for a greater variety of experiments, including multiple stages of mass analysis ( $MS^n$ ), without the addition of any hardware. The particle beam interface is better suited for coupling with an ion trap than is thermospray due to the high gas loads inherent to the thermospray process; the use of an external ion source with an ion trap would make this union more feasible.

The novel use of rapid removal of the RF trapping field to effect the ejection and detection of ions stored in a quadrupole ion trap has been examined. The application of a positive DC pulse to the ring electrode during the ejection period improved the observed ion signal by as much as hundred-fold for detection by this method. The use of a low frequency supplemental AC signal, which acts effectively as a DC pulse during the ion ejection time of 50-80  $\mu s$ , applied to the endcaps during the ejection period further improves the detected ion signal by approximately eight-fold. Overall, ejection by rapid removal of the RF produced a fifty-fold increase in detected ion signal as compared to the standard ejection method, mass-selective instability scanning. This technique is well suited for



efficiently detecting ions of a single mass-to-charge isolated in the ion trap (i.e., for SIM and SRM).

Future work in the on-line electrochemistry area could include extending these experiments to other compound classes. Carcinogen screening methods using ion-molecule reactions and tandem mass spectrometry have been developed in our laboratory, but these techniques are only applicable to direct-acting carcinogens. Using on-line electrochemistry in conjunction with ion/molecule reactions could provide a screening method for procarcinogens (species which require metabolic activation to produce the ultimate carcinogen) as well; the use of EC/MS to mimic metabolism has been demonstrated in previous work from our laboratory [17]. Also, design and implementation of a new on-line electrochemical cell could be a useful project. The current cells must be disposed of when the electrode becomes excessively fouled, and the cost of replacing the cell is significant. A cell which could be disassembled to allow for the use of a variety of working electrode materials and for the cleaning or replacement of dirty electrodes would be more convenient and cost-effective.

The examination of rapid removal of the RF as an ejection/detection technique is merely begun. Further experiments which demonstrate the use of this technique, and any improvements in factors such as limits of detection, in analytical applications should be undertaken. The use of rapid removal of RF in analyses which use selected ion monitoring (or selected reaction monitoring) should be examined to determine the analytical utility of the technique. Other fundamental aspects of the ion ejection process could also be examined through the use of more

sophisticated simulations and by extended examination of the various parameters to be optimized in the ejection process. Examination of other methods of causing ion ejection (e.g., resonant ejection or rapid increase in RF) could be useful in providing additional points of comparison for determining ion ejection efficiencies. An understanding of how this method can lead to a fifty-fold improvement in efficiency of ion ejection/detection could offer insight into the fate of ions which are not normally detected via mass-selective instability; if the mass-selective instability scan mode could be modified to detect these ions the enhanced sensitivity which results would be invaluable.

## LITERATURE CITED

1. Kim, H.Y.; Pilosof, D.; Dyckes, D.F.; Vestal, M.L. *J. Am. Chem. Soc.* **1984**, *105*, 7304.
2. Voyksner, R.D.; Pack, T. Proceedings of the 36th ASMS Conference on Mass Spectrometry and Allied Topics San Francisco, CA, **1988**, 1138.
3. Volk, K.J.; Yost, R.A.; Brajter-Toth, A. *J. Pharm. Biomed. Anal.* **1990**, *8*, 205.
4. Dryhurst, G. Electrochemistry of Biological Molecules; Academic Press: New York, **1977**.
5. Hawley, M.D.; Tatawawadi, S.V.; Piekarski, S.; Adams, R.N. *J. Am. Chem. Soc.* **1967**, *89*, 447.
6. Adams, R.N. *Anal. Chem.* **1976**, *48*, 1126A.
7. Neptune, M.; McCreery, R.L. *J. Org. Chem.* **1978**, *43*, 5006.
8. Bruckenstein, S.; Gadde, R.R. *J. Am. Chem. Soc.* **1971**, *93*, 793.
9. Bruckenstein, S.; Petek, M. *J. Electroanal. Chem.* **1973**, *42*, 397.
10. Bruckenstein, S.; Gadde, R.R. *J. Electroanal. Chem.* **1974**, *50*, 163.
11. Bolzan, A.E.; Iwasita, T.; Vielstich, W. *J. Electrochem. Soc.* **1987**, *134*, 3052.
12. Pinnick, W.J.; Lavine, B.K.; Weisenberger, C.R.; Anderson, L.R. *Anal. Chem.* **1980**, *52*, 1102.
13. Blakley, C.R.; Vestal, M.L. *Anal. Chem.* **1983**, *55*, 750.
14. Hambitzer, G.; Heitbaum, J. *Anal. Chem.* **1986**, *58*, 1067.
15. Mizoguchi, T.; Adams, R.N. *J. Am. Chem. Soc.* **1962**, *84*, 2058.
16. Galus, Z.; Adams, R.N. *J. Am. Chem. Soc.* **1962**, *84*, 2061.
17. Volk, K.J.; Yost, R.A.; Brajter-Toth, A. *Anal. Chem.* **1989**, *61*, 1709.
18. Rudewicz, P.; Straub, K.M. *Anal. Chem.* **1986**, *58*, 2928.
19. Perchalski, R.J.; Yost, R.A.; Wilder, B.J. *Anal. Chem.* **1982**, *54*, 1466.

20. Getek, T.A. Proceedings of the 35th ASMS Conference on Mass Spectrometry and Allied Topics Denver, CO, 1987, 443.
21. Bartmess, J.E.; Phillips, L.R. *Anal. Chem.* 1987, 59, 2014.
22. Paul, W.; Reinhard, H; von Zahn, V. *Z. Phys.* 1959, 156, 1.
23. Dawson, P.H. Quadrupole Mass Spectrometry and its Applications Elsevier: Amsterdam, 1976.
24. Yates, N.A.; Yost, R.A. Proceedings of the 39th ASMS Conference on Mass Spectrometry and Allied Topics Nashville, TN, 1991, 1489.
25. Covey, T.R.; Bruins, A.P.; Henion, J.D. *Org. Mass Spectrom.* 1988, 23, 178.
26. Alexander, A.J.; Kebarle, P. *Anal. Chem.* 1986, 58, 470.
27. Parker, C.E.; Smith, R.W.; Gaskell, S.J.; Bursey, M.M. *Anal. Chem.* 1986, 58, 1661.
28. Willoughby, R.C.; Browner, R.F. *Anal. Chem.* 1984, 56, 2626.
29. Kleintop, B.L. Ph.D. Dissertation, University of Florida, Gainesville, 1992.
30. Volk, K.J.; Yost, R.A.; Brajter-Toth, A. *Anal. Chem.* 1992, 64, 21A.
31. Volk, K.J.; Yost, R.A.; Brajter-Toth, A. *Anal. Chem.* 1989, 61, 1709.
32. Yates, N. A. Ph.D. Dissertation, University of Florida, Gainesville, 1992.
33. Eades, D.M.; Kleintop, B.L.; Yost, R.A. Proceedings of the 40th ASMS Conference on Mass Spectrometry and Allied Topics Washington, D.C., 1992, 1290.
34. Yates, N.A.; Griffin, T.P.; Yost, R.A. Proceedings of the 41st ASMS Conference on Mass Spectrometry and Allied Topics, San Francisco, CA, 1993, 444a.
35. Basic, C. Ph.D. Dissertation, University of Florida, Gainesville, 1992.
36. Brode, M.A. *J. Am. Chem. Soc.* 1955, 45, 1136.
37. Cooks, R.G. *Int. J. Mass Spectrom. Ion Processes* 1992, 118/119, 1.
38. Todd, J.F.J.; Waldren, R.M. *Int. J. Mass Spectrom. Ion Processes* 1979, 29, 301.
39. Mosburg, E.R. *Int. J. Mass Spectrom. Ion Processes* 1987, 77, 1.

40. Chien, B.M.; Michael, S.M.; Lubman, D.M. *Anal. Chem.* **1993**, 65, 1916.
41. Stafford, G.C.; Kelley, P.E.; Syka, J.E.P.; Reynolds, W.E.; Todd, J.F.J. *Int. J. Mass Spectrom. Ion Phys.* **1984**, 60, 85.
42. Jones, J.A.; Yost, R.A. Proceedings of the 42nd ASMS Conference on Mass Spectrometry and Allied Topics Chicago, IL, **1994**, 222.
43. Reiser, H.-P.; Julian, R.K.; Cooks, R.G. *Int. J. Mass Spectrom. Ion Processes*, **1992**, 121, 49.
44. Johnson, J.V.; Pedder, R.E.; Yost, R.A. *Rapid Commun. Mass Spectrom.* **1992**, 6, 760.
45. Eades, D.M. Ph.D. dissertation, University of Florida, Gainesville, 1993.

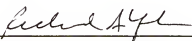
## BIOGRAPHICAL SKETCH

Jon Allen Jones was born on July 6, 1968 in Jacksonville, Florida. Jon lived briefly in Gainesville, Florida while his father completed his bachelor degree at the University of Florida. The Jones family then moved back to Jacksonville. Jon attended Edward H. White High School, where he met his future wife, and graduated in 1986.

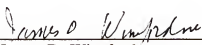
In August of 1986, Jon began attending Jacksonville University (JU). While at JU, Jon developed a love for chemistry and joined the university's Chemistry Society. On December 21, 1987, Jon married Michelle Bryant, his high school sweetheart. In April 1989, Jon earned his Bachelor of Science degree and decided to attend graduate school at the University of Florida.

In June 1990, Jon joined the research group of Dr. Richard A. Yost to conduct studies in ion trap mass spectrometry. The research was funded through grants from the US EPA. After 4 1/2 years of graduate work, Jon left Gainesville to teach at Florida Community College in Jacksonville (FCCJ) while completing his degree part-time. Upon completion of his graduate studies, Jon will begin work in the US Navy as a Nuclear Power Instructor in Orlando, Florida.

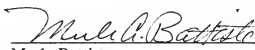
I certify that I have read this study and that in my opinion it conforms to acceptable standards of scholarly presentation and is fully adequate, in scope and quality, as a dissertation for the degree of Doctor of Philosophy.

  
Richard A. Yost, Chairman  
Professor of Chemistry

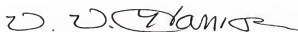
I certify that I have read this study and that in my opinion it conforms to acceptable standards of scholarly presentation and is fully adequate, in scope and quality, as a dissertation for the degree of Doctor of Philosophy.

  
James D. Winefordner  
Graduate Research Professor of Chemistry

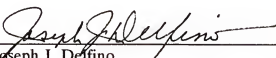
I certify that I have read this study and that in my opinion it conforms to acceptable standards of scholarly presentation and is fully adequate, in scope and quality, as a dissertation for the degree of Doctor of Philosophy.

  
Merle Battiste  
Professor of Chemistry

I certify that I have read this study and that in my opinion it conforms to acceptable standards of scholarly presentation and is fully adequate, in scope and quality, as a dissertation for the degree of Doctor of Philosophy.

  
Willard W. Harrison  
Professor of Chemistry

I certify that I have read this study and that in my opinion it conforms to acceptable standards of scholarly presentation and is fully adequate, in scope and quality, as a dissertation for the degree of Doctor of Philosophy.

  
\_\_\_\_\_  
Joseph J. Deffino  
Professor of Environmental Engineering Science

This dissertation was submitted to the Graduate Faculty of the Department of Chemistry in the College of Liberal Arts and Sciences and to the Graduate School and was accepted as partial fulfillment of the requirements for the degree of Doctor of Philosophy.

August 1995

\_\_\_\_\_  
Dean, Graduate School